8.A.8 Nuclear Physics B3 (1967) 469-503. North-Holland Publ. Comp., Amsterdam

EXPERIMENTAL RESULTS ON THE ($K\bar{K}$) AND (Kp) SYSTEMS AS OBSERVED IN THE ANNIHILATIONS $\bar{p}p \rightarrow K\bar{K}\pi$ AT REST

B. CONFORTO †, B. MARÉCHAL, L. MONTANET and M. TOMAS ††
CERN, Geneva

C. D'ANLAU, A. ASTIER, J. COHEN-GANOUNA and M. DELLA NEGRA
Laboratoire de Physique Nucléaire, Collège de France

M. BAUBILLIER, J. DUBOC, F. JAMES * and M. GOLDBERG
Institut de Physique Nucléaire, Paris

D. SPENCER
Nuclear Physics Research Laboratory, University of Liverpool, U.K.

Received 31 August 1967

Abstract: In the course of an extensive study of $\bar{p}p$ annihilations at rest involving $K\bar{K}$ pairs in the final state, 2000 events $\bar{p}p \rightarrow K_1^0 K^{\pm}\pi^{\mp}$ and 364 events $\bar{p}p \rightarrow K_1^0 K_1^0 \pi^0$ have been analyzed.

This analysis shows that the K*(891) is strongly produced. In addition, we observe a $K\bar{K}$ $J^P = 2^+$ resonance at 1280 MeV and a significant enhancement in the $K\bar{K}$ system at threshold, in $I = 1$. We also need S-wave ($K\pi$) amplitudes to reproduce the distribution of events on the Dalitz plot.

1. INTRODUCTION

In this article, we analyse the experimental results obtained on the three-body annihilations $\bar{p}p \rightarrow K\bar{K}\pi$ at rest.

These results correspond to a significant increase of the statistics compared with previous publications on the same subject (refs. [1, 2]).

They correspond to a total number of annihilations of 1.35×10^6 (the results we present here include the data discussed in ref. [1]).

The general analysis of the three-body $\bar{p}p \rightarrow K_1^0 K^{\pm}\pi^{\mp}$ will be presented in sect. 3 while sect. 4 will give the general results, which lead to the discus-

* Present address: CERN, Geneva.
† Now at the Enrico Fermi Institute, Chicago.
†† Now at Junta de Energia Nuclear, Madrid.

sion of four main topics: evidence for a new $K\bar{K}$ effect at threshold, presence of a small s-wave scattering length in the ($K\pi$) systems, presence of a ($K\bar{K}$) $J^P = 2^+$ resonance at 1280 MeV, properties of the K*(891) production. These four topics will be analysed in sects. 5, 6, 7 and 8 respectively.

In sect. 9, we shall compare the results obtained for the annihilations $\bar{p}p \rightarrow K_1^0 K_1^0 \pi^0$ to the properties of the annihilation $\bar{p}p \rightarrow K_1^0 K^{\pm}\pi^{\mp}$.

Let us recall that there are at least three good reasons to study the ($K\bar{K}$) and ($K\pi$) systems in three-body annihilations at rest; the final state is free from any reflection due to the presence of a baryonic particle; the initial state has well defined quantum numbers (since annihilations at rest occur mainly in $^1S_0$ and $^3S_1$ states); the limited number of particles in the final state allows a detailed analysis, using for instance the formalism developed by Zemach (ref. [3]).

In sect. 2, we describe the general procedure which has been followed for the identification of the events and their weighting.

2. TREATMENT OF THE DATA

1.35×10^6 antiprotons have been stopped in the 81 cm Saclay hydrogen bubble chamber, running at the CERN PS.

The antiprotons, produced in a beryllium target at 700 MeV/c, have been momentum and velocity analysed by means of the beam k4 (ref. [4]) and subsequently degraded by a 10 cm copper absorber down to 400 MeV/c just before entering the bubble chamber. The momentum of 400 MeV/c has been chosen so that the antiproton stoppings would occur near the middle of the bubble chamber.

A restricted fiducial volume has been chosen so as to reduce to $12 \pm 2\%$ the percentage of annihilations in flight before measurements and to ensure a high detection efficiency for the types of events analysed. Subsequently, a precise measurement of the incident track (the antiproton) (7 to 10 points measured on each of the three views on a length at least equal to 15 cm) lead to a further discrimination (prior to any kinematical analysis); it allowed to reduce the percentage of annihilations "in flight" to $6 \pm 2\%$. This percentage is still reduced when the kinematical fit is considered: it is of the order of 2% for the four-constraints fits ($\bar{p}p \rightarrow K_1^0 K^{\pm}\pi^{\mp}$) and of the order of 4% for the one-constraint fits ($\bar{p}p \rightarrow K_1^0 K_1^0 \pi^0$).

In any case, we have checked that our results are not significantly altered by the inclusion of 5% of annihilations in flight which are forced to simulate three-body annihilations at rest. We shall therefore take for granted that the small fraction of annihilations "in flight" which may be left in our sample of annihilations "at rest" does not affect significantly our results.

A double scan of the film shows that the scanning efficiency is of the order of 98% for events with V^0 particles far enough ($\geqslant 0.5$ cm) from the corresponding annihilations. To estimate the loss of events with V^0 decays close to the annihilation, we have used the distribution of the decay lengths of the observed V^0 particles. We have drawn this distribution for different momentum ranges of the V^0, using all the events of the same topology to increase our statistics.

Making use of the life-time of the K_1^0, we have then been able to assign to each event a weight depending on the momentum of the associated K_1^0. This weight takes also account of the losses due to the geometrical limitations of the chamber.

Fig. 1 shows the distribution of the weights as a function of the momentum of the K_1^0, averaged over all directions (this average affects only the part of the weight which depends on the geometrical limitations of the chamber. As it may be seen on fig. 1, this part of the weight is less important than the one due to the loss of V^0 decays close to the annihilation: it is negligeable for momenta smaller than 400 MeV/c).

We have checked that the weighted and unweighted distributions lead to the same interpretation. Therefore, in the following, we use the weights only for the determination of the annihilation rates.

$\bar{p}p \rightarrow K_1^0 K^{\pm}\pi^{\mp}$: These annihilations are to be found in the "two-prong-one-V^0" events, 15000 such events have been scanned and measured, of which 2000 are identified as $\bar{p}p \rightarrow K_1^0 K^{\pm}\pi^{\mp}$ annihilations at rest. One sees that the number of three-body events is small, compared to the total number of events with the same topology, most of them being four-body annihilations: $\bar{p}p \rightarrow K_1^0 K^{\pm}\pi^{\mp}\pi^0$ and $\bar{p}p \rightarrow K_1^0(K^0)\pi^+\pi^-$. However, the four-body contamination is found to be less than 1% after kinematical and ionization analysis. On the other hand, 2% of the good three-body annihilations are ambiguous between the two solutions $\bar{p}p \rightarrow K_1^0 K^+\pi^-$ and $\bar{p}p \rightarrow K_1^0 K^-\pi^+$. Since these events represent a small fraction of our sample, they are not included in the analysed data.

$\bar{p}p \rightarrow K_1^0 K_1^0 \pi^0$: These annihilations are to be found in the "zero-prong-two-V^0" events. 800 such events have been scanned and measured, of which 364 are identified as $\bar{p}p \rightarrow K_1^0 K_1^0 \pi^0$ annihilations at rest. In contrast with what happens for the charged three-body $\bar{p}p \rightarrow K_1^0 K^{\pm}\pi^{\mp}$, the neutral three-body $\bar{p}p \rightarrow K_1^0 K_1^0 \pi^0$ represent an important fraction of the total number of events with the same topology. The contamination of the three-body $\bar{p}p \rightarrow K_1^0 K_1^0 \pi^0$ into other annihilation channels ($\bar{p}p \rightarrow K_1^0 K_1^0 n\pi^0$ with $n > 1$) is then, a priori, very small. Moreover, it has been shown that the channel $\bar{p}p \rightarrow K_1^0 K_1^0$ is forbidden for annihilations at rest. The same quantum number arguments make it very likely that the channel $\bar{p}p \rightarrow K_1^0 K_1^0 \pi^0\pi^0$ is not open to annihilations at rest (ref. [5]). Therefore, the contamination of the three-body $\bar{p}p \rightarrow K_1^0 K_1^0 \pi^0$ could only come, eventually, from the five-body channel $\bar{p}p \rightarrow K_1^0 K_1^0 \pi^0\pi^0\pi^0$. This is very unlikely.

Fig. 2 shows the missing-mass spectrum for all events of the type $\bar{p}p \rightarrow K_1^0 K_1^0 M$ (where M is for 0, 1, or more neutral pions). It confirms the arguments given above and shows that in addition to the three-body $\bar{p}p \rightarrow K_1^0 K_1^0 \pi^0$ annihilations, these "zero-prong-two-V^0" events are mainly due to the channels $\bar{p}p \rightarrow K_1^0 K_1^0 \eta^0$ and $\bar{p}p \rightarrow K_1^0 K_1^0 \omega^0$.

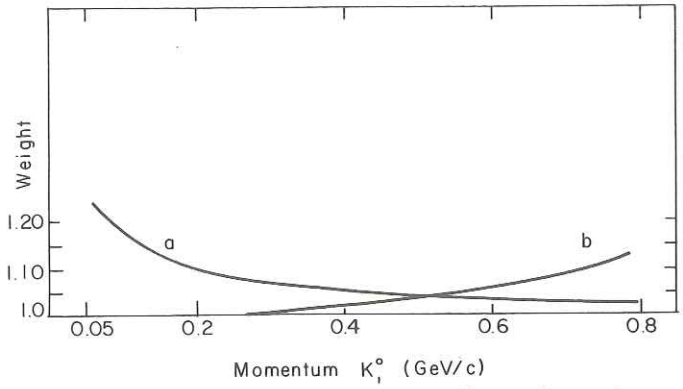

Fig. 1. Weighting of the events. The weight is given, for each event, as a function of the momentum of the associated K_1^o. This weight is the product of two terms, given by the curves (a) and (b). Curve (a) corresponds to the loss of K_1^o which decay closely to the annihilation: it affects mainly the small momenta. Curve (b) corresponds to the loss of K_1^o which escape from the visible volume of the chamber. This loss depends on the direction of the K_1^o. The curve gives an average loss, integrated on all directions.

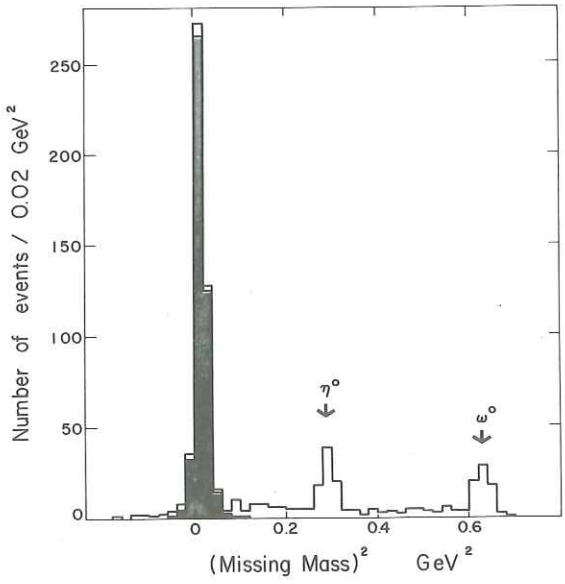

Fig. 2. Missing mass squared M for $\bar{p}p \rightarrow K_1^o K_1^o M$; M is for 0, 1 or more neutral pions. The three-body annihilations $\bar{p}p \rightarrow K_1^o K_1^o \pi^o$ are represented by the dark histogram. The remaining events are mainly concentrated around $M \sim \eta^o$ and $M \sim \omega^o$.

3. GENERAL METHOD USED FOR THE ANALYSIS OF THE THREE-BODY $\bar{p}p \rightarrow K\bar{K}\pi$

3.1. *Isospin analysis*

From the point of view of the isospin I and charge conjugation C, we have to consider four possible final states:

$$\bar{p}p \rightarrow K^0K^-\pi^+ , \quad \bar{p}p \rightarrow K^+\bar{K}^0\pi^- ,$$

$$\bar{p}p \rightarrow K^0\bar{K}^0\pi^0 , \quad \bar{p}p \rightarrow K^+K^-\pi^0 .$$

If the charge conjugation is conserved, the first two reactions correspond to the same process (ref. [6]).

As we only observe the charged decay mode of the K_1^0, $K_1^0 \rightarrow \pi^+\pi^-$, we shall only consider the four reactions:

$$\bar{p}p \rightarrow K_1^0K^{\pm}\pi^{\mp} , \tag{1}$$

$$\bar{p}p \rightarrow K_1^0K_1^0\pi^0 , \tag{2}$$

$$\bar{p}p \rightarrow K_1^0K_2^0\pi^0 , \tag{3}$$

$$\bar{p}p \rightarrow K^+K^-\pi^0 . \tag{4}$$

There are also four possible initial states corresponding to

$$C = \pm 1 , \quad I = 0, 1 .$$

The invariant transition amplitudes are obtained by projection of the final states with well defined charge conjugation $C = \pm 1$ on the four possible initial states. Using the relevant S-matrix elements:

$$S\,|\bar{p}p + \epsilon\bar{p}p\rangle = \sum_{I,i} A^{\epsilon}_{I,i}\,|\Phi^{\epsilon}_{I,i}\rangle , \tag{5}$$

with $\epsilon = \pm 1$ the charge conjugation eigenvalue, I the isospin of the total system, and i or $I_{K\bar{K}}$ the isospin of the K$\bar{K}$ system.
More explicitly: $A^{\epsilon}_{I,i} = \langle \Phi^{\epsilon}_{I,i}\,|\,S\,|\,p\bar{p} + \epsilon\bar{p}p\rangle$: transition amplitude

$$S\,|p\bar{p} + \epsilon\bar{p}p\rangle = A^{\epsilon}_{0,1}\,|\Phi^{\epsilon}_{0,1}\rangle + A^{\epsilon}_{1,0}\,|\Phi^{\epsilon}_{1,0}\rangle + A^{\epsilon}_{1,1}\,|\Phi^{\epsilon}_{1,1}\rangle ,$$

with

$$\Phi^{\epsilon}_{0,1} = \frac{1}{\sqrt{6}}\{[K^+\bar{K}^0\pi^- + K^0K^-\pi^+ - \frac{1}{\sqrt{2}}(K^+K^- + K^0\bar{K}^0)\pi^0]$$

$$+ \epsilon[K^-K^0\pi^+ + \bar{K}^0K^+\pi^- - \frac{1}{\sqrt{2}}(K^-K^+ + \bar{K}^0K^0)\pi^0]\} , \tag{6}$$

$$\Phi^{\epsilon}_{1,0} = \tfrac{1}{2}[(K^+K^- - K^0\bar{K}^0)\pi^0 + \epsilon(K^-K^+ - \bar{K}^0K^0)\pi^0] , \tag{7}$$

$$\Phi^{\epsilon}_{1,1} = \tfrac{1}{2}[(K^+\bar{K}^0\pi^- - K^0K^-\pi^+) + \epsilon(K^-K^0\pi^+ - \bar{K}^0K^+\pi^-)] . \tag{8}$$

Assuming the initial state is represented by an incoherent mixture of C

3. GENERAL METHOD USED FOR THE ANALYSIS OF THE THREE-BODY $\bar{p}p \to K\bar{K}\pi$

3.1. *Isospin analysis*

From the point of view of the isospin I and charge conjugation C, we have to consider four possible final states:

$$\bar{p}p \to K^0K^-\pi^+ , \quad \bar{p}p \to K^+\bar{K}^0\pi^- ,$$

$$\bar{p}p \to K^0\bar{K}^0\pi^0 , \quad \bar{p}p \to K^+K^-\pi^0 .$$

If the charge conjugation is conserved, the first two reactions correspond to the same process (ref. [6]).

As we only observe the charged decay mode of the K_1^0, $K_1^0 \to \pi^+\pi^-$, we shall only consider the four reactions:

$$\bar{p}p \to K_1^0K^{\pm}\pi^{\mp} , \tag{1}$$

$$\bar{p}p \to K_1^0K_1^0\pi^0 , \tag{2}$$

$$\bar{p}p \to K_1^0K_2^0\pi^0 , \tag{3}$$

$$\bar{p}p \to K^+K^-\pi^0 . \tag{4}$$

There are also four possible initial states corresponding to

$$C = \pm 1 , \quad I = 0, 1 .$$

The invariant transition amplitudes are obtained by projection of the final states with well defined charge conjugation $C = \pm 1$ on the four possible initial states. Using the relevant S-matrix elements:

$$S\,|\bar{p}p + \epsilon\bar{p}p\rangle = \sum_{I,i} A^{\epsilon}_{I,i}\,|\Phi^{\epsilon}_{I,i}\rangle , \tag{5}$$

with $\epsilon = \pm 1$ the charge conjugation eigenvalue, I the isospin of the total system, and i or $I_{K\bar{K}}$ the isospin of the $K\bar{K}$ system.
More explicitly: $A^{\epsilon}_{I,i} = \langle \Phi^{\epsilon}_{I,i}\,|S\,|p\bar{p} + \epsilon\bar{p}p\rangle$: transition amplitude

$$S\,|p\bar{p} + \epsilon\bar{p}p\rangle = A^{\epsilon}_{0,1}\,|\Phi^{\epsilon}_{0,1}\rangle + A^{\epsilon}_{1,0}\,|\Phi^{\epsilon}_{1,0}\rangle + A^{\epsilon}_{1,1}\,|\Phi^{\epsilon}_{1,1}\rangle ,$$

with

$$\Phi^{\epsilon}_{0,1} = \frac{1}{\sqrt{6}}\{[K^+\bar{K}^0\pi^- + K^0K^-\pi^+ - \frac{1}{\sqrt{2}}(K^+K^- + K^0\bar{K}^0)\pi^0]$$

$$+ \epsilon[K^-K^0\pi^+ + \bar{K}^0K^+\pi^- - \frac{1}{\sqrt{2}}(K^-K^+ + \bar{K}^0K^0)\pi^0]\} , \tag{6}$$

$$\Phi^{\epsilon}_{1,0} = \tfrac{1}{2}[(K^+K^- - K^0\bar{K}^0)\pi^0 + \epsilon(K^-K^+ - \bar{K}^0K^0)\pi^0] , \tag{7}$$

$$\Phi^{\epsilon}_{1,1} = \tfrac{1}{2}[(K^+\bar{K}^0\pi^- - K^0K^-\pi^+) + \epsilon(K^-K^0\pi^+ - \bar{K}^0K^+\pi^-)] . \tag{8}$$

Assuming the initial state is represented by an incoherent mixture of C

eigenstates, and using the following notation for the transition rates:

$$R_1 = |\langle \bar{p}p|S|K_1^0 K^{\pm}\pi^{\mp}\rangle|^2 , \qquad R_2 = |\langle \bar{p}p|S|K_1^0 K_1^0 \pi^0\rangle|^2 ,$$

$$R_3 = |\langle \bar{p}p|S|K_1^0 K_2^0 \pi^0\rangle|^2 , \qquad R_4 = |\langle \bar{p}p|S|K^+ K^- \pi^0\rangle|^2 ,$$

we obtain

$$R_1 = \tfrac{1}{9}|\sqrt{2}A^+_{0,1} + \sqrt{3}\,A^+_{1,1}|^2 + \tfrac{1}{9}|\sqrt{2}A^-_{0,1} + \sqrt{3}\,A^-_{1,1}|^2 , \tag{9}$$

$$R_2 = \tfrac{1}{27}|A^+_{0,1} + \sqrt{3}A^+_{1,0}|^2 , \tag{10}$$

$$R_3 = \tfrac{1}{9}|A^-_{0,1} + \sqrt{3}A^-_{1,0}|^2 , \tag{11}$$

$$R_4 = \tfrac{1}{6}|A^+_{0,1} - \sqrt{3}A^+_{1,0}|^2 + \tfrac{1}{6}|A^-_{0,1} - \sqrt{3}A^-_{1,0}|^2 . \tag{12}$$

In these rates, we have introduced the branching ratio

$$\frac{\Gamma(\pi^0\pi^0)}{\Gamma(\pi^+\pi^-)} = \frac{1}{2} ,$$

for the K_1^0, since we only observe the charged decay mode $K_1^0 \to \pi^+\pi^-$.

In this formulation, we have used the decomposition $(K\bar{K}, \pi)$. It is of course possible to use another decomposition. The Racah recoupling coefficients allow to go from one decomposition to the other one in a simple way: If Φ and φ refer to the decomposition $(K\bar{K}, \pi)$ and $(K\pi, \bar{K})$ respectively:

$$\Phi^{\epsilon}_{0,1} = \varphi^{\epsilon}_{0,\frac{1}{2}} , \tag{13}$$

$$\Phi^{\epsilon}_{1,0} = -\frac{1}{\sqrt{3}}\varphi^{\epsilon}_{1,\frac{1}{2}} + \sqrt{\tfrac{2}{3}}\,\varphi^{\epsilon}_{1,\frac{3}{2}} , \tag{14}$$

$$\Phi^{\epsilon}_{1,1} = -\sqrt{\tfrac{2}{3}}\,\varphi^{\epsilon}_{1,\frac{1}{2}} - \frac{1}{\sqrt{3}}\,\varphi^{\epsilon}_{1,\frac{3}{2}} . \tag{15}$$

In the appendix, we present the decomposition according to the $K\pi$ coupling scheme. It leads directly to the above relations (13), (14) and (15).

For the following discussion, it is interesting to point out that $\Phi^{\epsilon}_{1,1}$ is a superposition of $I(K\pi) = \frac{1}{2}$ states $(\varphi_{1,\frac{1}{2}})$ and $I(K\pi) = \frac{3}{2}$ states $(\varphi_{1,\frac{3}{2}})$.

3.2. *Symmetry properties of the amplitudes in the space variables*

We prefer the use of the first decomposition $(K\bar{K}, \pi)$ which corresponds to amplitudes with well defined symmetry properties in the exchange of the space variables of the K and the $\bar{K}$.

This is a consequence of the G-parity conservation. The G-parity of a $K\bar{K}$ system of isospin $I(K\bar{K})$, and relative orbital angular momentum $l(K\bar{K})$ is given by:

$$G(K\bar{K}) = (-1)^{I(K\bar{K})+ l(K\bar{K})}. \quad (16)$$

On the other hand the G-parity of the $\bar{p}p$ system is equal to

$$G(\bar{p}p) = \epsilon(-1)^I = G(K\bar{K}) \times G(\pi) . \quad (17)$$

That leads to the symmetry properties given in table 1a.

Table 1a
Symmetry properties of the amplitudes $A_{I,i}$

Amplitudes	$G(\bar{p}p)$	$G(K\bar{K})$	$l(K\bar{K})$
A^{+}_{01}	+	-	even
A^{-}_{01}	-	+	odd
A^{+}_{10}	-	+	even
A^{-}_{10}	+	-	odd
A^{+}_{11}	-	+	odd
A^{-}_{11}	+	-	even

These symmetry properties may also be found in the expressions of the wave functions $\Phi^{\epsilon}_{I,i}$ as expected from the symmetrization postulate: by definition, conservation of C and I leads to G-conservation. More precisely, the symmetry properties of the $\Phi^{\epsilon}_{I,i}$ states in the exchange of the internal variables of the K, $\bar{K}$ particles are given in table 1b.

Table 1b
Symmetry properties of the amplitudes $\Phi_{I,i}$

Amplitude	Φ^{+}_{01}	Φ^{-}_{01}	Φ^{+}_{10}	Φ^{-}_{10}	Φ^{+}_{11}	Φ^{-}_{11}
Symmetry in the internal variables of the K, $\bar{K}$	even	odd	even	odd	odd	even

3.3. *Partial wave decomposition*

(a) *Definitions*: Let us start with a simple non-relativistic description. Fig. 3 gives the definition of the variables which will be used: $i = 1, 2, 3$, corresponds to the particles K, $\bar{K}$, π; $\boldsymbol{p}_i$ is the momentum of the particle i; $\boldsymbol{p}_{jk} = (m_j\boldsymbol{p}_k - m_k\boldsymbol{p}_j)/(m_j + m_k)$ the relative momentum of particles j and k; and $\cos\theta_{jk} = \hat{p}_{jk} \cdot \hat{p}_i$, where $\hat{p}_{jk} = \boldsymbol{p}_{jk}/|\boldsymbol{p}_{jk}|$ and $\hat{\boldsymbol{p}}_i = \boldsymbol{p}_i/|\boldsymbol{p}_i|$.

We define also: J, the total angular momentum; l_{jk}, the relative orbital momentum between particles j and k; and L_i, the relative orbital momentum between particle i and the (jk) system.

Since $\epsilon = +1$ corresponds to the $^1S_0$ initial state ($C = +1$, $J = 0$) and $\epsilon = -1$ corresponds to the $^3S_1$ initial state ($C = -1$, $J = +1$), we can rewrite $A^{\epsilon}_{I,i}$ as $A^{J}_{I,i}$.

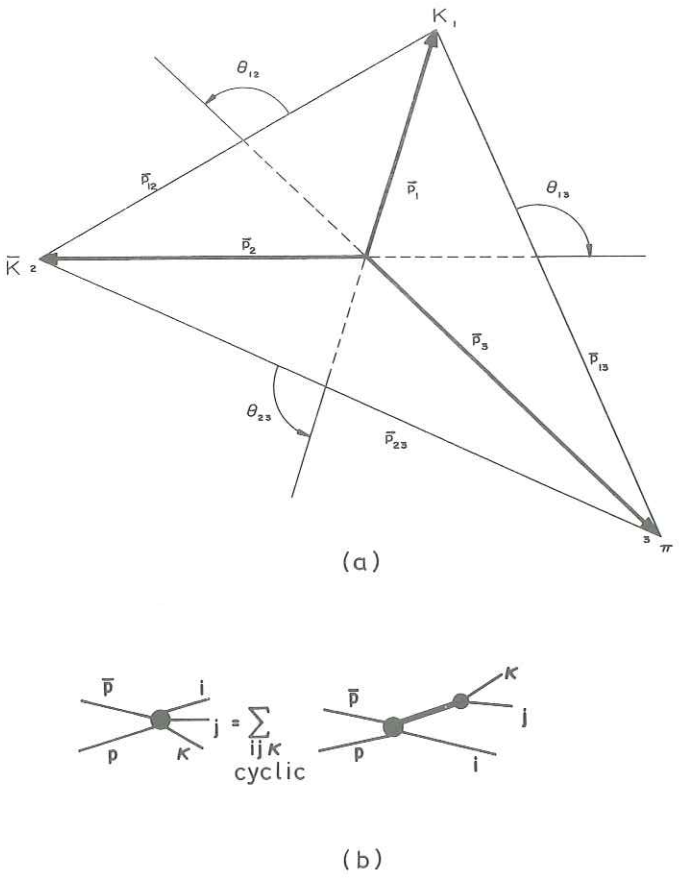

Fig. 3. (a) Wick triangle showing the relations between the momenta p_i ($i=1,2,3$) of the three particles, in the total centre-of-mass system, the relative momenta p_{ij} and the angles θ_{jk} used for the partial-wave decomposition. (b) Diagram showing the two-body decomposition of the three-body annihilations, as it is used in our model.

(b) *Multiple final state interaction model*: We shall assume that the three-body annihilation process $\bar{p}p \rightarrow K\bar{K}\pi$ can be described by the terms appearing in the development shown on fig. 3b. With this model, we assume that the final state interactions are much stronger than the single production term (ref. [7]). Furthermore, for each term, we suppose the energy dependence of the total phase of the annihilation amplitude is given by the phase δ_{jk} of the (j,k) scattering in the angular momentum state l_{jk} and the isospin state I_{jk}.

We choose as independent dynamical variables for the jk coupling s_{jk} the invariant mass squared of the jk system and θ_{jk}.

We obtain:

$$A^J_{I,I_{12}} = \sum_{L_3, l_{12}} a^J_{L_3 l_{12}}(s_{12}, \theta_{12}) \frac{e^{i\delta_{12}} \sin \delta_{12}}{p_{12}}$$

$$+ \sum_{L_2, l_{13}, I_{13}} b_{L_2 l_{13}}(s_{13}, \theta_{13}) \frac{e^{i\delta_{13}} \sin \delta_{13}}{p_{13}}$$

$$+ \sum_{L_1, l_{23}, I_{23}} c^J_{L_1 l_{23}}(s_{23}, \theta_{23}) \frac{e^{i\delta_{23}} \sin \delta_{23}}{p_{23}} \,. \qquad (18)$$

(c) *Selection rules*: The negative parity of the initial state imposes $L_i = l_{jk}$. The G-parity imposes that each amplitude $A_{I,I_{12}}$ is even or odd in the exchange of the space variable of the K (cf. sect. 3.2). We must have:

$$A^J_{I,I_{K\overline{K}}} = \sum_{\substack{l \text{ even} \\ \text{odd}}} a^J_{ll}(s_{K\overline{K}}, \theta_{K\overline{K}}) \frac{e^{i\delta_{K\overline{K}}} \sin \delta_{K\overline{K}}}{p_{K\overline{K}}} \qquad (19)$$

$$+ \sum_{\lambda, I_{K\pi}} [b_{\lambda\lambda}(s_{K\pi}, \theta_{K\pi}) \frac{e^{i\delta_{K\pi}} \sin \delta_{K\pi}}{p_{K\pi}} \pm b_{\lambda\lambda}(s_{\overline{K}\pi}, \theta_{\overline{K}\pi}) \frac{e^{i\delta_{\overline{K}\pi}} \sin \delta_{\overline{K}\pi}}{p_{\overline{K}\pi}}].$$

3.4. *Separation of the angular variables*

Making use of symmetric, traceless cartesian tensors $T^{i_1 \ldots i_l}(\hat{p})$ $i_1, \ldots, i_l = 1, 2, 3$ constructed on the unit three-vectors $\hat{p}$ which define the directions of the relative impulsions corresponding to the decomposition l_{jk}, L_i (ref. [3]) for the representations of the angular momentum l, we write $a_{ll}{}^J$ or $b_{ll}{}^J$:

$$a^J_{ll} = \rho^l(s_{jk}) f(\theta_{jk}) \,,$$

where $\rho^l(s_{jk})$ is a scalar function of s_{jk} and $f(\theta_{jk})$ is given by

$$f = T^{i_1 \ldots i_l}(\hat{p}_{jk}) T^{i_1 \ldots i_l}(\hat{p}_i) \qquad \text{when } J = 0 \,,$$

$$f = S^m \epsilon^{mii'} T^{ii_1 \ldots i_{l-1}}(\hat{p}_{jk}) T^{i'i_1 \ldots i_{l-1}}(\hat{p}_i) \quad \text{when } J = 1 \,,$$

S^m ($m = 1, 2, 3$) represents the spin-1 of the initial state, $\epsilon^{mii'}$ is the completely antisymmetric tensor with three indices ($\epsilon^{123} = +1$).

3.5. *Approximations introduced for the energy-dependent part of the amplitude*

The amplitudes are then of the form

$$\rho^I(s_{jk}) \frac{\epsilon^{i\delta_{jk}} \sin \delta_{jk}}{p_{jk}} f(\theta_{jk}) , \tag{20}$$

with $f(\theta_{jk}) = T^I(\hat{p}_{jk}) : T^I(\hat{p}_i)$.

The scalar function $\rho^I \, e^{i\delta_{jk}} \sin \delta_{jk}/p_{jk}$ must satisfy the following threshold conditions:

$$\text{when } p_{jk} \to 0, \quad \rho^l \frac{e^{i\delta_{jk}} \sin \delta_{jk}}{p_{jk}} \approx c^{te} \, p_{jk}^l$$

$$\text{when } p_i \to 0, \quad \rho^l \frac{e^{i\delta_{jk}} \sin \delta_{jk}}{p_{jk}} \approx c^{te} \, p_i^l \quad , \tag{21}$$

and to describe a resonance, we use the Breit-Wigner formula. For instance, for the K*(891) resonance produced on a p-wave, the energy dependence of the amplitude will be given by the formula:

$$\frac{c^{te} \, p_{K\pi} p_K}{m_{K\pi}^2 - m_o^2 + i\Gamma m_o} \tag{22}$$

where Γ, the width, is taken as a constant, However, for a resonance near threshold, we shall use the formula (29). We shall also make use of the scattering length in the zero range approximation, to describe an interaction near threshold: for instance, for the $K\pi$ system near threshold produced on an s-wave

$$\frac{c^{te}}{1 - iap_{K\pi}} . \tag{23}$$

With these definitions, each amplitude is determined but to a complex constant which is left as a free complex parameter in the fitting procedure.

Although we have given, for simplicity, a non-relativistic description of the general method of analysis, our results are given, in the following, in terms of relativistic matrix elements.

4. GENERAL EXPERIMENTAL RESULTS FOR $\bar{p}p \to K_1^0 K^{\pm} \pi^{\mp}$

Fig. 4 shows the production Dalitz plot for the reaction $\bar{p}p \to K_1^0 K^{\pm} \pi^{\mp}$. This Dalitz plot may be qualified by the following remarks:

(i) A noticeable asymmetry, with respect to the first diagonal, which is an evidence for the presence of interference effects between the amplitudes of the two isospin states $I = 0$, $I = 1$. More precisely, if we define two regions in the Dalitz-plot by the inequalities:

Region I : $M^2(K\pi)^0 > M^2(K\pi)^{\pm}$,

Region II : $M^2(K\pi)^0 < M^2(K\pi)^{\pm}$,

the densities are then:

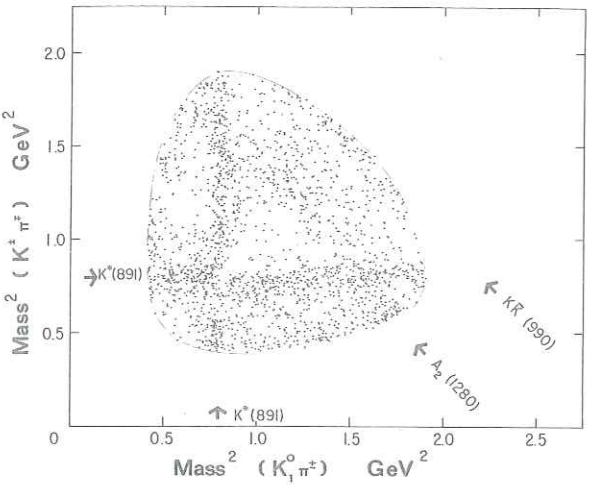

Fig. 4. Effective-mass squared Dalitz plot for $\bar{p}p \to K^{o}_{1}K^{\pm}\pi^{\mp}$ (2000 events). Four accumulations of events are visible: the $K^{*o}(891)$, $K^{*+}(891)$, $K\bar{K}(1280)$ and $K\bar{K}(990)$. They are indicated by the arrows.

$$R(\mathrm{I}) = \tfrac{1}{9}\left|\sqrt{2}\, A^{+(\mathrm{I})}_{0,1} + \sqrt{3}\, A^{+(\mathrm{I})}_{1,1}\right|^2 + \tfrac{1}{9}\left|\sqrt{2}\, A^{-(\mathrm{I})}_{0,1} + \sqrt{3}\, A^{-(\mathrm{I})}_{1,1}\right|^2$$

$$R(\mathrm{II}) = \tfrac{1}{9}\left|\sqrt{2}\, A^{+(\mathrm{I})}_{0,1} - \sqrt{3}\, A^{+(\mathrm{I})}_{1,1}\right|^2 + \tfrac{1}{9}\left|-\sqrt{2}\, A^{-(\mathrm{I})}_{0,1} + \sqrt{3}\, A^{-(\mathrm{I})}_{1,1}\right|^2.$$

On the folded Dalitz plot (fig. 5), the density is given by the sum of the

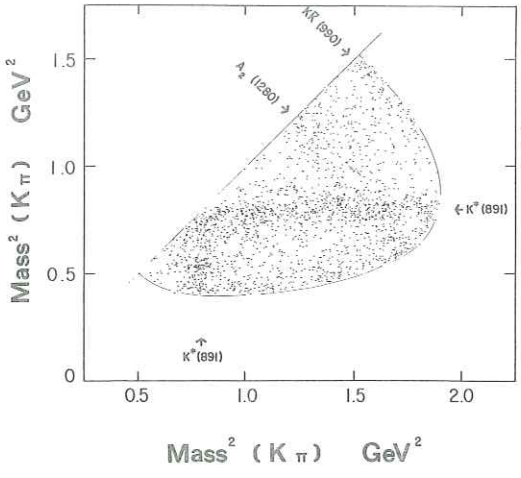

Fig. 5. Folded Dalitz plot for $\bar{p}p \to K^{o}_{1}K^{\pm}\pi^{\mp}$.

contributions of the four amplitudes: $A^{+}_{0,1}$, $A^{+}_{1,1}$, $A^{-}_{0,1}$ and $A^{-}_{1,1}$:

$$R(\mathrm{I+II}) = \tfrac{4}{9}|A^{+}_{0,1}|^2 + \tfrac{2}{3}|A^{+}_{1,1}|^2 + \tfrac{4}{9}|A^{-}_{0,1}|^2 + \tfrac{1}{3}|A^{-}_{1,1}|^2 . \qquad (26)$$

The interference effects disappear.

(ii) An accumulation of events in the two K*(891) regions, the $K^{*\pm}$ being less abundant than the K^{*0} (figs. 6 and 7). The decay angular distributions of the K* (figs. 8 and 9) do not correspond to a pure $\sin^2\theta$ or $\cos^2\theta$ distribution, as it would be the case if all K* were produced in a pure $^3S_1$ or $^1S_0$ annihilation state.

(iii) A sharp peaking of events near the $K\bar{K}$ threshold (fig. 10). This peaking is even more striking when we concentrate our attention on the events for which both ($K\pi$) effective mass squared are larger than 0.9 GeV^2 (the main purpose of this cut is to remove the K* contribution) (fig. 11). Fig. 12 shows the decay angular distribution of the $K\bar{K}$ system for $M^2(K\bar{K}) < 1.08$ GeV^2: it is compatible with isotropy.

(iv) An accumulation of events in the ($K\bar{K}$) system around 1280 MeV. This accumulation is seen, both on the complete sample (fig. 10) and on the selected one (fig. 11).

Fig. 13 shows the decay angular distribution of the $K\bar{K}$ system in the 1280 MeV region: the presence of the charged K*($\cos\theta \approx -0.6$) and of the neutral K*($\cos\theta \approx 0.6$) contribute to its anisotropy.

(v) In addition to the contributions of the K* and of the $K\bar{K}$ enhancements at threshold and at 1280 MeV, we still observe a non-uniform density of events which may be characterized by a hole in the middle of the Dalitz plot and a small but significant increase towards the ($K\pi$) threshold energies. We have obtained a good interpretation of these observations with the introduction of S-wave amplitudes represented by a scattering length, for the ($K\pi$) systems.

Taking into account these qualitative facts, we have attempted to interpret the complete distribution of the Dalitz-plot, using the general method developed in sect. 3.

We use the following definitions:

$g^{\mu\nu}$: metric tensor 1, -1, -1, -1;

p^{μ}_{K1}, p^{μ}_{K2}, p^{μ}_{π}: four-momentum vectors for K^0_1, $K^{\pm}$, $\pi^{\mp}$;

$E^{\mu} = p^{\mu}_{K1} + p^{\mu}_{K2} + p^{\mu}_{\pi}$: total four-momentum vector;

$s_{K1\pi} = (p_{K1} + p_{\pi})^2$: invariant mass squared for $(K^0_1\pi^{\pm})$;

$s_{K2\pi} = (p_{K2} + p_{\pi})^2$: invariant mass squared for $(K^{\pm}\pi^{\mp})$;

$s_{K1K2} = (p_{K1} + p_{K2})^2$: invariant mass squared for $(K^0_1K^{\pm})$;

$\bar{p}^{\mu}_{K1} = p^{\mu}_{K1} - E^{\mu}(E_{\nu}\cdot p^{\nu}_{K1}/E^2)$, i.e. $(0, p_{K1})$ in the total rest frame;

$\bar{p}^{\mu}_{K2} = p^{\mu}_{K2} - E^{\mu}(E_{\nu}\cdot p^{\nu}_{K2}/E^2)$, i.e. $(0, p_{K2})$ in the total rest frame;

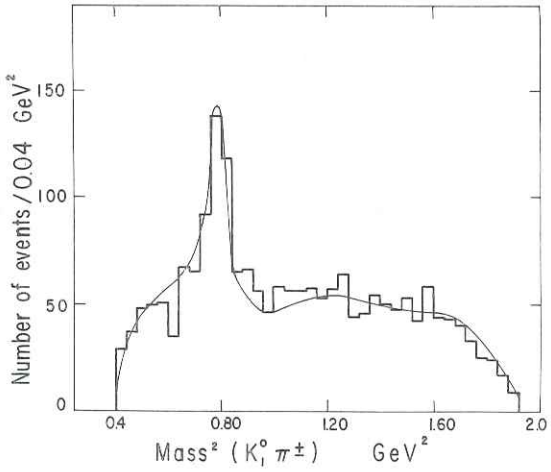

Fig. 6. $(K^0_1\pi^\pm)$ effective mass squared distribution for $\bar{p}p \rightarrow K^0K^\pm\pi^\mp$. The curve represents the theoretical distribution as given by the best fit (solution (iii) of table 2). The $K^{*\pm}(891)$ is clearly visible.

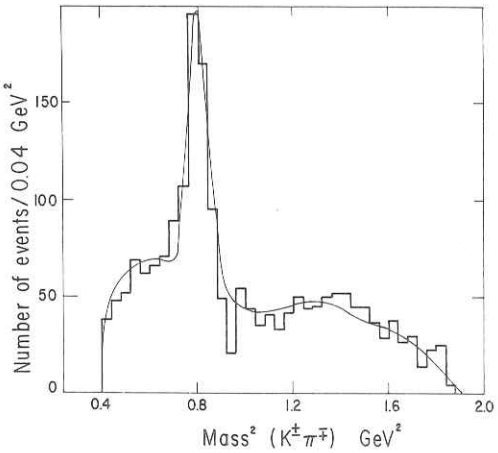

Fig. 7. $(K^\pm\pi^\mp)$ effective mass squared distribution for $\bar{p}p \rightarrow K^0_1K^\pm\pi^\mp)$. The curve represents the theoretical distribution as given by the best fit (solution (iii) of table 2). The $K^{*0}(891)$ is clearly visible.

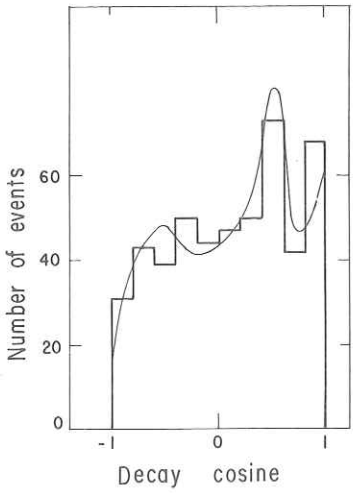

Fig. 8. Decay angular distribution of the $K^{*\pm}(891) \rightarrow K^0_1\pi^\pm$ in $\bar{p}p \rightarrow K^0_1K^\pm\pi^\mp$. The curve represents the theoretical distribution as given by the best fit (solution (iii) of table 2).

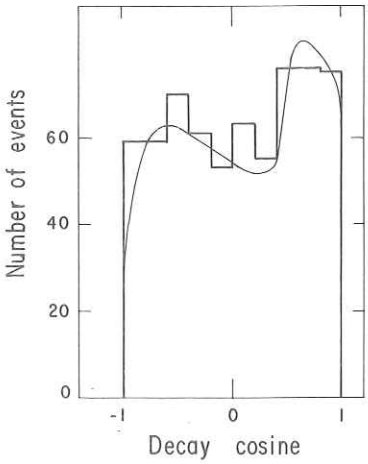

Fig. 9. Decay angular distribution of the $K^{*0}(891) \rightarrow K^\pm\pi^\mp$ in $\bar{p}p \rightarrow K^0_1K^\pm\pi^\mp$. The curve represents the theoretical distribution as given by the best fit (solution (iii) of table 2).

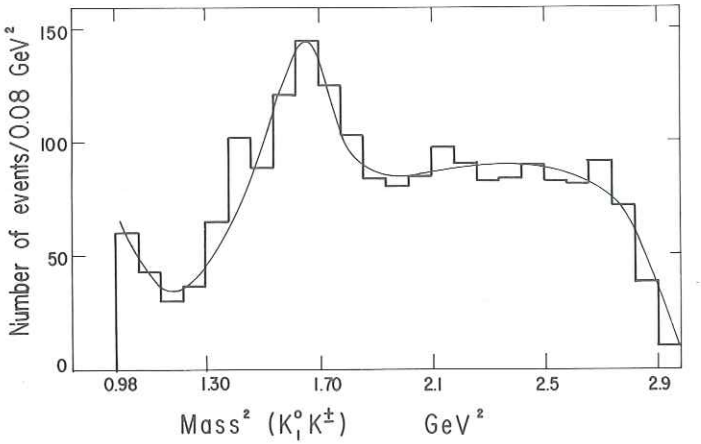

Fig. 10. $(K^0_1K^\pm)$ effective mass squared distribution for $\bar{p}p \rightarrow K^0_1K^\pm\pi^\mp$. The curve corresponds to the theoretical distribution as given by the best fit (solution (iii) of table 2). The accumulations of events at 990 MeV and at 1280 MeV (effective mass squared of 0.98 and 1.64 GeV^2) are clearly visible.

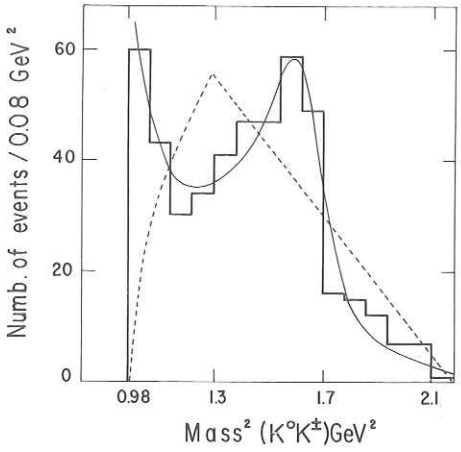

Fig. 11. $(K_1^0K^{\pm})$ effective mass squared for $\bar{p}p \to K_1^0K^{\pm}\pi^{\mp}$ when $M^2(K\pi) > 0.9$ GeV^2. This cut is to remove the K*(891) contribution. The full curve corresponds to the theoretical distribution as given by the best fit (solution (iii) of table 2). The dashed curve represents the phase space. The accumulations of events at 990 MeV and at 1280 MeV are clearly visible.

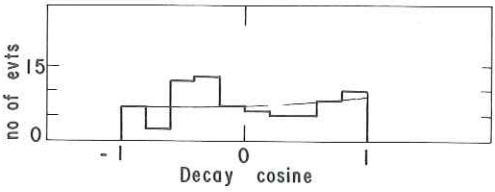

Fig. 12. Decay angular distribution of the KK̄ system for $M^2(K\bar{K}) < 1.08$ GeV^2 in $\bar{p}p \to K_1^0K^{\pm}\pi^{\mp}$. The curve represents the theoretical distribution as given by the best fit (solution (iii) of table 2).

$\bar{p}_\pi^\mu = p_\pi^\mu - E^\mu(E_\nu \cdot p_\pi^\nu/E^2)$, i.e. $(0, p_\pi)$ in the total rest frame;

$p_{K_1\pi}^\mu = (p_\pi - p_{K1})^\mu - [(m_\pi^2 - m_{K1}^2)/s_{K_1\pi}](p_\pi + p_{K1})^\mu$, i.e. $(0, \boldsymbol{p}_\pi - \boldsymbol{p}_{K1})$ in the $(K_1\pi)$ rest frame;

$p_{K_2\pi}^\mu = (p_\pi - p_{K2})^\mu - [(m_\pi^2 - m_{K2}^2)/s_{K_2\pi}](p_\pi + p_{K2})^\mu$, i.e. $(0, \boldsymbol{p}_\pi - \boldsymbol{p}_{K2})$ in the $(K_2\pi)$ rest frame;

$p_{K1K2}^\mu = (p_{K2} - p_{K1})^\mu - [(m_{K2}^2 - m_{K1}^2)/s_{K1K2}](p_{K1} + p_{K2})^\mu$, i.e. $(0, \boldsymbol{p}_{K2} - \boldsymbol{p}_{K1})$ in the (K_1K_2) rest frame.

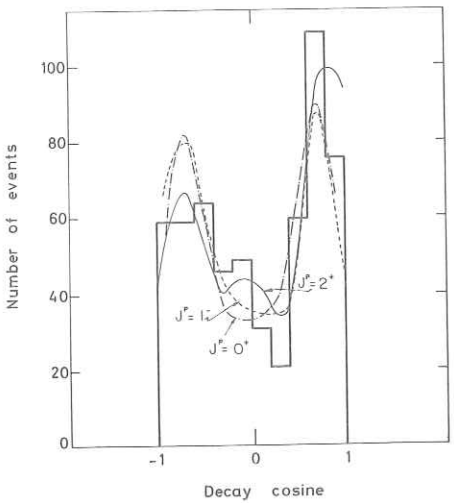

Fig. 13. Decay angular distribution of the $K\bar{K}(1280)$ in $\bar{p}p \to K_1^0 K^{\pm}\pi^{\mp}$. The three curves represent the theoretical distributions as given by the fit for different spin-parity assignments. The best fit corresponds to spin-parity 2^+.

These four-vectors are the relativistic generalization of the vectors $\boldsymbol{p}_{ij}$ and $\boldsymbol{p}_K$ considered in sect. 3.

We now give the explicit form of the amplitudes $A^+_{0,1}$, $A^+_{1,1}$, $A^-_{0,1}$ and $A^-_{1,1}$ which govern the reaction (1).

(i) The amplitude $A^+_{0,1}$ corresponds to ${}^1S_0$, $I=0$ initial state. We have to consider the contributions of the K*(891), the $K\bar{K}(1280)$, the $K\bar{K}$ at threshold and the $(K\pi)$ S-wave in $I_{K\pi} = \frac{1}{2}$.

a) K*(891); $J^P = 1^-$,

$$\frac{p^{\mu}_{K_1\pi}\bar{p}_{K_2\mu}}{s_{K_1\pi} - s_{K^*} + i\sqrt{s_{K^*}}\,\Gamma_{K^*}} + \frac{p^{\mu}_{K_2\pi}\bar{p}_{K_1\mu}}{s_{K_2\pi} - s_{K^*} + i\sqrt{s_{K^*}}\,\Gamma_{K^*}} \,. \tag{27}$$

b) $K\bar{K}(1280)$; $J^P = 2^+$,

$$\frac{T^{\mu\nu}(p_{K1K2})\,T_{\mu\nu}(\bar{p}_{\pi})}{s_{K1K2} - s_{A_2} + i\sqrt{s_{A_2}}\,\Gamma_{A_2}} \,,$$

where

$$T^{\mu\nu}_{(p_{K1K2})} = p^{\mu}_{K1K2}\,p^{\nu}_{K1K2} - \tfrac{1}{3}\left(g^{\mu\nu} - \frac{(p_{K1}+p_{K2})^{\mu}(p_{K1}+p_{K2})^{\nu}}{s_{K1K2}}\right)p^2_{K1K2} \,,$$

$$T^{\mu\nu}_{(\bar{p}_{\pi})} = \bar{p}^{\mu}_{\pi}\bar{p}^{\nu}_{\pi} - \tfrac{1}{3}\left(g^{\mu\nu} - \frac{E^{\mu}E^{\nu}}{E^2}\right)p^2_{\pi} \,.$$

c) K$\bar{K}$(1000); $J^P = 0^+$,

$$\frac{1}{s_{K1K2} - s_0 + ip_{K1K2}\gamma} . \tag{29}$$

In the limit of a narrow resonance far from threshold, this width γ may be related to the more classical "constant width" Γ by the relation

$$\Gamma = p_{K1K2}\gamma/\sqrt{s_0} .$$

d) Kπ (S-wave; $I_{K\pi} = \frac{1}{2}$) ,

$$\frac{1}{1 - ia_{\frac{1}{2}}\sqrt{-p^2_{K_1\pi}}} + \frac{1}{1 - ia_{\frac{1}{2}}\sqrt{-p^2_{K_2\pi}}} . \tag{30}$$

(ii) The amplitude $A^+_{1,1}$ corresponds to $^1S_0$, $I=1$ initial state. We have to consider the contribution of the K*(891), the K$\bar{K}$(1280) and of the (Kπ) S-waves in $I_{K\pi} = \frac{1}{2}$ and $I_{K\pi} = \frac{3}{2}$.

a) K*(891); $J^P = 1^-$,

$$\frac{p^{\mu}_{K_1\pi}\bar{p}_{K_2\mu}}{s_{K_1\pi} - s_{K^*} + i\sqrt{s_{K^*}}\,\Gamma_{K^*}} - \frac{p^{\mu}_{K_2\pi}\bar{p}_{K_1\mu}}{s_{K_2\pi} - s_{K^*} + i\sqrt{s_{K^*}}\Gamma_{K^*}} . \tag{31}$$

b) Kπ (S-wave, $I_{K\pi} = \frac{1}{2}$) ,

$$\frac{1}{1 - ia_{\frac{1}{2}}\sqrt{-p^2_{K_1\pi}}} - \frac{1}{1 - ia_{\frac{1}{2}}\sqrt{-p^2_{K_2\pi}}} . \tag{32}$$

c) Kπ (S-wave, $I_{K\pi} = \frac{3}{2}$) ,

$$\frac{1}{1 - ia_{\frac{3}{2}}\sqrt{-p^2_{K_1\pi}}} - \frac{1}{1 - ia_{\frac{3}{2}}\sqrt{-p^2_{K_2\pi}}} . \tag{33}$$

(iii) The amplitude $A^-_{0,1}$ corresponds to $^3S_1$, $I=0$ initial state; only K*(891) will contribute

$$\epsilon_{\mu\nu\rho\sigma} p^{\nu}_{K_1} p^{\rho}_{K_2} p^{\sigma}_{\pi} \left[\frac{1}{s_{K_1\pi} - s_{K^*} + i\sqrt{s_{K^*}}\,\Gamma_{K^*}} + \frac{1}{s_{K_2\pi} - s_{K^*} + i\sqrt{s_{K^*}}\,\Gamma_{K^*}}\right], \tag{34}$$

where $\epsilon_{\mu\nu\rho\sigma}$ is the completely antisymmetric tensor with four indices ($\epsilon_{0123} = +1$) .

(iv) The amplitude $A^-_{1,1}$ corresponds to $^3S_1$, $I=1$ initial state.

a) K*(891); $J^P = 1^-$,

$$\epsilon_{\mu\nu\rho\sigma} p^{\nu}_{K1} p^{\rho}_{K2} p^{\sigma}_{\pi} \left[\frac{1}{s_{K_1\pi} - s_{K^*} + i\sqrt{s_{K^*}}\,\Gamma_{K^*}} + \frac{1}{s_{K_2\pi} - s_{K^*} + i\sqrt{s_{K^*}}\,\Gamma_{K^*}} \right]. \quad (35)$$

b) $K\bar{K}(1280)$; $J^P = 2^+$,

$$\epsilon_{\mu\nu\rho\sigma} p^{\nu}_{K1} p^{\rho}_{K2} p^{\sigma}_{\pi} (p_{K1K2}\, \bar{p}_{\pi\tau}) \frac{1}{s_{K_1K_2} - s_{A_2} + i\sqrt{s_{A_2}}\,\Gamma_{A_2}} . \quad (36)$$

Each amplitude $A^{+}_{0,1}$, $A^{+}_{1,1}$, $A^{-}_{0,1}$ and $A^{-}_{1,1}$ is a linear combination of the above contributions, each of them being introduced with a complex parameter $\rho_K \exp(i\varphi_K)$ to be fitted with the data.

We assume no interference effects between the amplitude corresponding to $^3S_1$ and $^1S_0$ initial states. Therefore, absorbing the Clebsch-Gordan coefficients in the parameters $\rho_K \exp(i\varphi_K)$, the expression to be fitted to the density distribution is of the form:

$$R = |A^{+}_{0,1} + A^{+}_{1,1}|^2 + |A^{-}_{0,1} + A^{-}_{1,1}|^2 \quad (37)$$

The 10 contributions described above lead then to a fit of 17 real parameters (disposing of an overall normalization factor and of a phase for each of the initial states $^3S_1$, and $^1S_0$).

The Dalitz plot has been divided into 192 cells (0.1 $GeV^2 \times 0.1$ GeV^2).

As it will be explained in sects. 5 and 6, we have been led to proceed to three different least square fittings corresponding to the following parametrizations:

(i) a Breit-Wigner parametrization for the $K\bar{K}(1000)$ and $a_{\frac{3}{2}}(K\pi) = -a_{\frac{1}{2}}(K\pi)$

(ii) a Breit-Wigner parametrization for the $K\bar{K}(1000)$ and $a_{\frac{3}{2}}(K\pi) = 0$

(iii) a scattering length parametrization for the $K\bar{K}(1000)$ and $a_{\frac{3}{2}}(K\pi) = -a_{\frac{1}{2}}(K\pi) = -0.3$ fm.

The results are given in table 2.

The distribution of the cells for which the contribution to the χ^2 is large does not show a systematic arrangement on the Dalitz plot, but for the interference regions of the K* and the $K\bar{K}(1280)$ resonances. It gives us confidence in the fits obtained for the general features of the amplitudes introduced in these fits, in particular for the masses, widths and scattering lengths, as well as for the intensities ρ^2, but indicates that the phases φ, quoted in table 2 may be subject to large errors.

This table 2 gives, for each solution, the values obtained for the parameters and the corresponding number of events to be attributed to each contribution (given by the integration of the squared modulus of the amplitudes).

In this fitting procedure the masses, widths and scattering lengths have been kept constant.

In a second step, the best values for these quantities have been obtained with a fit where all the physical quantities were kept constant, but one.

One may notice that the total number of events obtained when adding all the contributions is not equal to the total number of events: this is due to some of the interferences for which the integral over the Dalitz plot is not zero.

Table 2
The parameters ρ and φ

Solution (i), $\chi^2 = 260$. $\langle\chi^2\rangle = 175$. $a_{\frac{3}{2}} \neq 0$

Channel	Amplitude	ρ	φ	Number of events	
K*		0.61	0.00[a])	216	K*^{0}. M=890 MeV, Γ=45 MeV
S-wave Kπ $I_{K\pi}=\frac{1}{2}$	A^+_{01}	0.96	0.60	534	K*$^\pm$. M=895 MeV, Γ=45 MeV
K$\bar{K}$(1280)		0.67	1.02	260	
K$\bar{K}$(1000)		0.27	2.68	42	K$\bar{K}$(1280). M=1280 MeV, Γ=90 MeV
K*		0.23	-0.80	30	K$\bar{K}$(1000). M=1016 MeV. γ=200 MeV
S-wave Kπ $I_{K\pi}=\frac{1}{2}$	A^+_{11}	0.58	1.84	191	
S-wave Kπ $I_{K\pi}=\frac{3}{2}$		0.71	-1.74	290	$a_{\frac{1}{2}}$(Kπ) = 0.3 fm
K*	A^-_{11}	1.00[a])	0.00[a])	580	$a_{\frac{3}{2}}$(Kπ) = -0.3 fm
K$\bar{K}$(1280)		0.26	3.07	41	
K*	A^-_{01}	0.22	1.11	28	

Solution (ii) $\chi^2 = 258$, $\langle\chi^2\rangle = 177$, $a_{\frac{3}{2}} = 0$

Channel	Amplitude	ρ	φ	Number of events	
K*		0.60	0.00[a])	190	K*^{0}; M=887 MeV, Γ=40 MeV
S-wave Kπ $I_{K\pi}=\frac{1}{2}$	A^+_{01}	1.11	1.79	650	K*$^\pm$; M=897 MeV, Γ=40 MeV
K$\bar{K}$(1280)		0.68	1.00	247	
K$\bar{K}$(1000)		0.28	2.91	40	K$\bar{K}$(1280); M=1280 MeV, Γ=90 MeV
K*	A^+_{11}	0.31	5.24	51	K$\bar{K}$(1000); M=1016 MeV, γ=200MeV
S-wave Kπ $I_{K\pi}=\frac{1}{2}$		0.64	5.87	214	$a_{\frac{1}{2}}$(Kπ) = -0.4 fm
K*	A^-_{11}	1.00[a])	0.00[a])	526	$a_{\frac{3}{2}}$(Kπ) = 0
K$\bar{K}$(1280)		0.30	3.04	48	
K*	A^-_{01}	0.16	0.98	14	

a) One module set to +1, two phases set to zero.

Table 2 (continued)

Solution (iii), $\chi^2 = 262$, $\langle\chi^2\rangle = 175$. $K\bar{K}(1000)$: scattering length					
Channel	Amplitude	ρ	φ	Number of events	
K*		0.63	0.00[a])	210	K^{*0}; M=890 MeV, Γ=45 MeV
S-wave $K\pi$ $I_{K\pi}=\frac{1}{2}$	A^{+}_{01}	1.40	0.36	1033	$K^{*\pm}$; M=895 MeV, Γ=45 MeV
$K\bar{K}(1280)$		0.71	1.27	264	
$K\bar{K}(1000)$		0.95	2.01	475	$K\bar{K}(1280)$; M=1280 MeV, Γ=90 MeV
K*		0.23	-0.04	28	$K\bar{K}(1000)$: $a_{0(K\bar{K})} = 2$ fm
S-wave $K\pi$ $I_K = \frac{1}{2}$	A^{+}_{11}	0.64	1.26	218	
S-wave $K\pi$ $I_{K\pi} = \frac{3}{2}$		0.38	-1.78	75	$a_{\frac{1}{2}}(K\pi) = 0.3$ fm
K*	A^{-}_{11}	1.00[a])	0.00[a])	530	$a_{\frac{3}{2}}(K\pi) = -0.3$ fm
$K\bar{K}(1280)$		0.31	3.08	52	
K*	A^{-}_{01}	0.37	1.28	72	

[a]) One module set to +1, two phases set to zero.

5. $K\bar{K}$ STRUCTURE AROUND 1000 MeV

The accumulation of events observed for the $(K^0_1K^{\pm})$ system near 1000 MeV (figs. 10 and 11) does not correspond to a well-known phenomenon. However, the same observation is made for other annihilation channels ($\bar{p}p \rightarrow K^0_1K^{\pm}\pi^{\mp}\pi^{+}\pi^{-}$ at rest, (ref. [8]), $\bar{p}p \rightarrow K^0_1K^{\pm}\pi^{\mp}\pi^0$ at 1.2 GeV/c (ref. [9]), $\bar{p}p$ annihilations into 4, 5 and 6 particles at 3.7 GeV/c (ref. [10])). In the three-body $\bar{p}p \rightarrow K^0_1K^{\pm}\pi^{\mp}$ we are now analysing, the effect is more important and deserves a detailed study.

First of all, we have made sure this accumulation at the edge of the Dalitz-plot is not due to misidentified or badly measured events which could be forced, by kinematical constraints to simulate a three-body annihilation with minimum mass for the $(K\bar{K})$ system. Indeed, the Dalitz plot of the three-body events still shows the $(K\bar{K})$ threshold accumulation when the measured quantities are used instead of the fitted ones.

In a first approach, we have tried to interpret this accumulation by the presence of strong interference effects in the $(K\pi)$ S-wave amplitudes $I_{K\pi}=\frac{1}{2}$ and $I_{K\pi}=\frac{3}{2}$. As can be seen in table 3, none of the attempted solutions give an acceptable interpretation of the data.

When the scattering lengths $a_{\frac{1}{2}}$ and $a_{\frac{3}{2}}$ have comparable values, the $(K\pi)I_{K\pi}=\frac{1}{2}$ and $I_{K\pi}=\frac{3}{2}$ amplitudes corresponding to the $^1S_0$, $I=1$ initial state have the same energy dependence, and are therefore indistinguishable.

Table 3
Results of the first approach

$a_{\frac{1}{2}}$	$a_{\frac{3}{2}}$	χ^2	$a_{\frac{1}{2}}$	$a_{\frac{3}{2}}$	χ^2
0.0	-0.4	525	-0.2	0.0	395
0.0	-0.2	469	-0.2	0.2	459
0.0	0.2	444	-0.2	0.4	418
0.0	0.4	426	-0.4	0.0	477
0.2	-0.4	478	-0.4	0.2	420
0.2	-0.2	476	-0.4	0.4	429
0.2	0.0	434			
0.4	-0.4	428			
0.4	-0.2	453			
0.4	0.0	477			

$\langle \chi^2 \rangle = 177.$

Table 3 gives the χ^2 obtained when $a_{\frac{1}{2}}$ and $a_{\frac{3}{2}}$ are sufficiently different. For scattering lengths smaller than 0.4 fm or larger than -0.4 fm, there is no solution.

As expected, the main contribution to the badness of the fit comes from the excess of events in the (KK̄) threshold region (fig. 14).

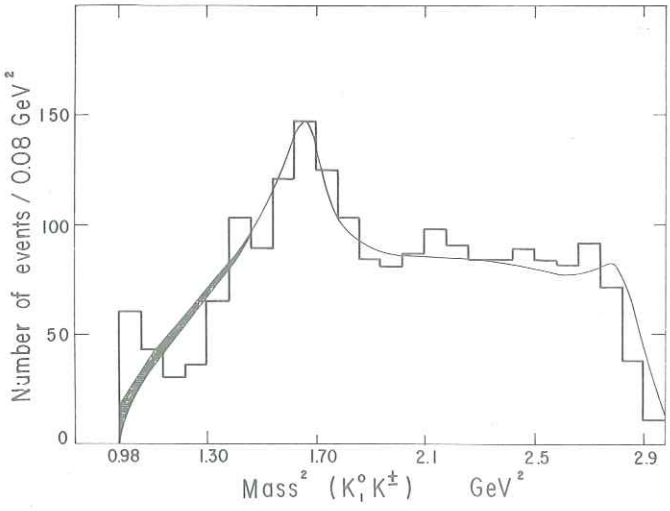

Fig. 14. ($K^0_1K^{\pm}$) effective mass squared spectrum for $\bar{p}p \rightarrow K^0_1K^{\pm}\pi^{\mp}$. The curves represent the theoretical distributions as given by the fit when no KK̄ threshold effect is introduced. The curves are in good agreement with the experimental data for effective mass squared sufficiently far from the threshold region. Near threshold, the hatched region corresponds to the domain of expected distributions for different values of $a_{\frac{1}{2}}$ and $a_{\frac{3}{2}}$ (the S-wave scattering length of the (Kπ) systems). It is clear that none of these curves is in good agreement with the data near threshold.

Therefore, we must introduce an additional amplitude to take into account of the ($K\bar{K}$) threshold effect. We present first the results obtained when this amplitude is parametrized in terms of one real parameter, namely a scattering length a_0 in the zero effective range approximation. We shall then discuss the results obtained when the parametrization of the ($K\bar{K}$) amplitude is done in terms of two real parameters, s_0 and γ, as it is the case for the Breit-Wigner formulation.

We have fixed the scattering lengths $a_{\frac{1}{2}}$ and $a_{\frac{3}{2}}$ to $a_{\frac{1}{2}} = 0.3$ fm, $a_{\frac{3}{2}} = -0.3$ fm, although the parameters a_0, (s_0, γ) characterizing the ($K\bar{K}$) effect near threshold are correlated to the numerical values chosen for $a_{\frac{1}{2}}$ and $a_{\frac{3}{2}}$; these values for $a_{\frac{1}{2}}$ and $a_{\frac{3}{2}}$ gave us the best interpretation of the Dalitz plot distribution and are therefore preferred to any other set, for a discussion of the $K\bar{K}$ structure at threshold.

(i) *Introduction of a real scattering length.* The ($K\bar{K}$) amplitude is approximated, near threshold, by

$$\frac{1}{1 - ia_0 p_{K1K2}} .$$

Table 4 shows the results obtained for several values of a_0.

Table 4
Values of χ^2 for different a_0

a_0 (fm)	χ^2_D	$\chi^2_{K\bar{K}(1)}$	$\chi^2_{K\bar{K}(2)}$	a_0 (fm)	χ^2_D	$\chi^2_{K\bar{K}(1)}$	$\chi^2_{K\bar{K}(2)}$
0.0	389	134	125				
0.4	286	39.6	44	-0.4	323	65.8	47.6
1.0	266	26.5	24.8	-1.0	287	37.0	34.0
2.0	262	21.0	17.0	-2.0	266	27.0	15.0
3.0	264	19.9	15.9	-3.0	266	24.6	13.5
4.0	266	19.4	15.7	-4.0	267	23.6	13.5
6.0	274	22.0	16.7	-6.0	268	23.0	13.7
10.0	274	21.0	17.3	-10.0	270	22.8	14.0
20.0	278	23.0	18.9				

where χ^2_D means χ^2 on the Dalitz plot ($\langle\chi^2_D\rangle = 175$), $\chi^2_{K\bar{K}(1)}$ means χ^2 on the ($K\bar{K}$) effective mass squared spectrum ($\langle\chi^2_{K\bar{K}(1)}\rangle = 25$), $\chi^2_{K\bar{K}(2)}$ means χ^2 on the ($K\bar{K}$) effective mass squared spectrum when K* contributions are excluded ($M^2(K\pi) \geq 0.9\,\mathrm{GeV}^2$) ($\langle\chi^2_{K\bar{K}(2)}\rangle = 16$).

The curve SL on fig. 15 represents the distribution expected for the solution $a_0 = 2$ fm ($\chi^2/\langle\chi^2\rangle = 17/16$). As it can be seen on table 4 and fig. 16, the

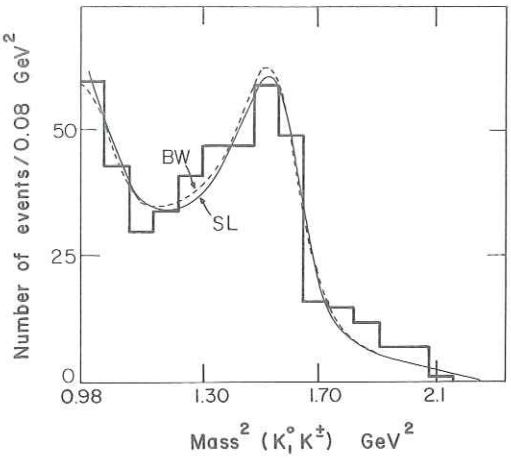

Fig. 15. $(K_1^0 K^{\pm})$ effective mass squared distribution for $\bar{p}p \to K_1^0 K^{\pm} \pi^{\mp}$ when $M^2(K\pi) > 0.9\ \mathrm{GeV}^2$. Curve SL represents the theoretical distribution as given by the fit when an S-wave scattering length of 2 fm is introduced for the $K\bar{K}$ threshold effect.

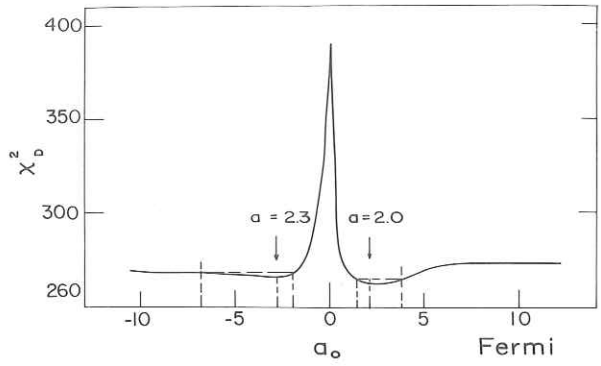

Fig. 16. $\chi^2_D = f(a_0)$, a_0 being a real scattering length introduced to interpret the $K\bar{K}$ enhancement at threshold. Two solutions are acceptable: $a_0 = 2.0\ ^{+\ 1.0}_{-\ 0.5}$ fm which corresponds to a marked minimum for the χ^2_D value, and $a_0 = -2.3\ ^{+\ 0.3}_{-\ 4.0}$ fm, which has no well defined lower limit ($\Delta a_0 = 4$ fm) but leads to an interesting interpretation of the $K\bar{K}$ enhancement (see text).

scattering length formulation leads to two possible solutions, with rougly the same absolute value for a_0, but with opposite signs:

$$a_0 = 2.0\ ^{+\ 1.0}_{-\ 0.5}\ \mathrm{fm}, \quad a_0 = -2.3\ ^{+\ 0.3}_{-\ 4.0}\ \mathrm{fm}\ .$$

Although $a_0 \approx 2$ fm is not a very large scattering length, the curve SL reproduces quite well the sharp variation of the density near threshold owing to the strong destructive interference effects between the $K\bar{K}$ amplitude and the S-wave $K\pi$, $I = \frac{1}{2}$ amplitude.

(ii) *Introduction of a Breit-Wigner amplitude.* To represent the $K\bar{K}$ amplitude near threshold in terms of two real parameters, we have introduced the complex Breit-Wigner amplitude:

$$\frac{1}{s_{K\bar{K}} - s_0 + ip_{K\bar{K}}\gamma} .$$

The following mass and width are obtained:

$$\sqrt{s_0} = m_0 = 1016 \pm 6 \text{ MeV} ,$$

$$\gamma = 200 \pm 40 \text{ MeV} .$$

This width γ corresponds to a "classical width" $\Gamma \approx 25$ MeV, Γ being defined by the relation

$$\Gamma = \frac{p_{K\bar{K}}\gamma}{m_0} .$$

We have discussed in sect. 4 the validity of such a relation.

The curve BW on fig. 15 represents the distribution expected for this solution.

The three solutions presented in table 2 correspond to a production of 42, 40 and 475 events, respectively, for the $K\bar{K}$ threshold enhancement.

These figures correspond to production rates of the order of 10^{-5} to 10^{-4}, differing by a factor 10, but as we have seen strong interferences with S-wave $K\pi$ amplitudes may be present, leading to large errors on the estimation of the production rate of the $K\bar{K}$ threshold enhancement.

Although, from the above discussion, the nature of the $K\bar{K}$ enhancement observed at threshold is not clear, it may be interesting to consider, at least, the following possible interpretations:

a) The $I = 1$ $K\bar{K}$ channel is dominated, in this energy region, by an amplitude represented by a positive real scattering length of 2 fm which may correspond to a virtual state.

b) The $K\bar{K}$ enhancement is due to the presence of a resonance with $m_0 \approx$ 1016 MeV and $I^G J^P = 1^- 0^+$. The spin-parity assignment is suggested by the position of this resonance near threshold and the decay angular distribution of the $K\bar{K}$ system (fig. 12).

With these assignments, it is impossible to identify this resonance with the φ, S*, H^0 or $\delta^\pm$ mesons. We must therefore assume in this case that this is a new object, which can also decay into $\eta\pi$. No such object has yet been observed.

(c) The $I = 1$ $K\bar{K}$ channel is dominated, at threshold, by a virtual bound state resonance (ref. [11]). This resonance may be coupled to the $\eta\pi$ channel. To take into account this possibility, we have tried a fit with a complex scattering length $a_0 + ib_0$. The result, $b_0 = 0^{+0.5}_{-0}$ fm suggests that the partial width of this resonance in the $\eta\pi$ channel is probably quite narrow. In these

conditions, the value $a_0 = -2.3$ fm corresponds to a narrow $\eta\pi$ resonance with mass $m = 872$ MeV.

If this interpretation is correct, it is tempting to identify this narrow $\eta\pi$ resonance, at 972 MeV, to the relatively well established δ-meson. This approach of the δ-meson with a structure in the $I=1$ $K\overline{K}$ system was first suggested by Dalitz (ref. [12]), who took the opposite approach and asked what $I = 1$ $K\overline{K}$ threshold scattering length $(a + ib)$ would correspond to the mass and width reported for the δ-meson and found $a = -1.6$ fm and $b < 0.1$ fm, in good agreement with our direct analysis of the $K\overline{K}$ structure.

Then, our results lead to the following quantum number assignments for the δ-meson: $I^G J^P = 1^- 0^+$. However, this interpretation seems to present a difficulty if one takes seriously the indication that the width of this scalar resonance should be relatively small while the $\eta\pi$ channel is kinematically opened. If, for some unexplained reason, the strong $\eta\pi$ decay mode was depressed, the electromagnetic decays would be in competition.

6. THE S-WAVE (Kπ) AMPLITUDES

In addition to the concentrations of events in the regions: $K\overline{K}(1000)$, $K\overline{K}(1280)$, and $K\pi(891)$, we observe a distribution of events which suggest that the $^3S_1$ initial state does not contribute to the background, since the central region of the Dalitz plot is empty (for $^3S_1$, the density should be maximum in this region). Indeed, we observe a non-uniform distribution characterized by a slow decrease of the density when we go from the edges of the Dalitz-plot to the centre.

A good interpretation of this effect is given by the introduction of S-wave scattering lengths in the (Kπ) systems.

Since the $^3S_1$ initial state does not lead to S-wave (Kπ) amplitudes, we have just to consider the two possible initial states $^1S_0$ ($I=0$, $I=1$). For the final states, we consider the $I = \frac{1}{2}$ and $I = \frac{3}{2}$ (Kπ) state.

The appropriate amplitudes have been described in sect. 4.

The two amplitudes corresponding to the initial state $^1S_0$, $I=1$, for $I(K\pi) = \frac{1}{2}$ and $I(K\pi) = \frac{3}{2}$, are represented by the same function if $a_{\frac{1}{2}} \approx a_{\frac{3}{2}}$. We therefore consider two possibilities:

(i) The two amplitudes are almost undistinguishable ($a_{\frac{1}{2}} \approx a_{\frac{3}{2}}$) and we introduce a single term for these amplitudes, in the fitting procedure, with a phenomenological scattering length a. The results are not very sensitive to the value chosen for a. The best results are obtained for $a \approx -0.4$ fm, they correspond to the solution (ii) of table 2.

(ii) The two amplitudes have a different energy dependence ($a_{\frac{1}{2}} = -a_{\frac{3}{2}}$). The results are, again, not very sensitive to the value chosen for $a_{\frac{1}{2}}$. The best results are obtained for

$$a_{\frac{1}{2}} = 0.3 \text{ fm}, \qquad a_{\frac{3}{2}} = -0.3 \text{ fm} .$$

They correspond to the solution (i) of table 2.

Whichever solution is chosen for the S-wave ($K\pi$) amplitudes, the whole results remain essentially the same with respect to the $K\bar{K}(1280)$ and $K^*(891)$ resonances. We are therefore able, with our model, to investigate in more detail the production of the $K\bar{K}(1280)$ and $K^*(891)$ resonances.

7. THE ($K\bar{K}$) STRUCTURE AROUND 1280 MeV

Figs. 10 and 11 show an accumulation of events in the ($K\bar{K}$) system around 1280 MeV. Fig. 13 shows the decay angular distribution of the ($K\bar{K}$) system around 1280 MeV; its strong anisotropy does not necessarily mean that the spin of the ($K\bar{K}$) resonance is different from zero, since strong interference effects may be present, in particular with the $K^*(891)$ and the S-wave ($K\pi$) amplitudes.

Table 5 gives the results of the fit obtained for different spin-parity assignments.

Table 5
Results of the fit for different spin-parity of $K\bar{K}(1280)$

$J^P(K\bar{K})$	$\chi^2(1)$	$\chi^2(2)$
0^+	355	33
1^-	340	26
2^+	260	19

In table 5, $\chi^2(1)$ is the χ^2 of the fit of the Dalitz plot ($\langle \chi^2(1) \rangle = 177$), $\chi^2(2)$ is the χ^2 of the fit of the angular distribution in the $K\bar{K}(1280)$ region as shown on fig. 13 ($\langle \chi^2(2) \rangle = 10$).

The three curves given on fig. 13 represent the angular distributions expected for the spin-parity 0^+, 1^-, 2^+; $J^P = 2^+$ is favoured over 1^- and 0^+.

The central value for the mass has been fitted as described in sect. 4, with the following result:

$$M = 1280 \pm 12 \text{ MeV}.$$

The best fit is obtained for a width of 90 MeV.

In fig. 11, the $K\bar{K}(1280)$ enhancement is significantly displaced towards the low mass values. The fit gives a good interpretation of this phenomenon, which is due to interference effects.

The two initial states $^3S_1$ and $^1S_0$ contribute to the production of the $K\bar{K}(1280)$ resonance: taking an average value between the three solutions presented in table 2 (the difference between the three solutions, from this point of view, is small compared to statistical errors), we find that 257 ± 40 events are produced by annihilations in $^1S_0$ state and 47 ± 20 events are produced by annihilations in $^3S_1$ state.

Taking into account the $K^0_2K^\pm$ decay mode of the $(K\bar{K})^\pm$ resonance, the

non-observation of the $K_1^0 \to 2\pi^0$ decay mode and an average weight of 1.14 for scanning and geometrical losses, the rate of annihilation into the channel $pp \to (K\overline{K})^{\pm}\pi^{\mp}$ is then

$$304 \times 2 \times 1.5 \times 1.14 \times \frac{1}{1.15 \times 10^6} = (9 \pm 3) \times 10^{-4} .$$

The results obtained for the mass, the width and the spin make it probable that this object is a manifestation of the so-called $A_2(1300)$ meson.

8. THE K*(891) PRODUCTION

The Dalitz-plot (fig. 4) shows an abundant production of K*(891). Both $^1S_0$ and $^3S_1$ may contribute to this production: indeed, the decay angular distributions of the K*(891) show, at least qualitatively, that both initial state contribute. Moreover, the interference between the two K* appears to be strongly destructive and indicates that the $I=1$ initial state is preponderant in the K* production.

We have given in sect. 4 the explicit expressions for the four amplitudes corresponding to the initial states $^1S_0$ ($I=0$, $I=1$) and $^3S_1$ ($I=0$, $I=1$).

Table 6 gives the production rates obtained for average over the three solutions given in table 2.

Table 6
Production rates for $\bar{p}p \to K^*\overline{K}(\overline{K}^*K)$

Initial state	Observed events	Events produced	Rates
$^1S_0\ I=0$	205 ± 30	950 ± 150	$f_{K^*K}^{+0} = 8.4 \times 10^{-4} \pm 1.4 \times 10^{-4}$
$^1S_0\ I=1$	36 ± 7	150 ± 35	$f_{K^*K}^{+1\ \text{antisym}} = 1.3 \times 10^{-4} \pm 0.3 \times 10^{-4}$
$^3S_1\ I=0$	38 ± 25	200 ± 125	$f_{K^*K}^{-0} = 1.7 \times 10^{-4} \pm 1.0 \times 10^{-4}$
$^3S_1\ I=1$	546 ± 50	2650 ± 250	$f_{K^*K}^{-1\ \text{sym}} = 23.4 \pm 2.0 \times 10^{-4}$

The $^3S_1$, $I=1$ initial state is preponderant for the production of the K*(891). However, the contribution of $^1S_0$, $I=0$ is not negligible.

One notices that the ratio $[\bar{p}p \to K^*K(^1S_0)]/[\bar{p}p \to K^*K(^3S_1)]$ is close to $\frac{1}{3}$. Then the theoretical decay angular distributions of the K* are expected to be $3 \times 0.5 \sin^2\theta + \cos^2\theta$ which is almost uniform. The theoretical curves corresponding to the best fit drawn on figs. 8 and 9 are effectively uniform apart from interference effects between the two K* and in good agreement with the experimental distributions.

It is possible to extract from these results (making use of the relative phase between the $I=0$ and $I=1$ K* production amplitudes) the number of events for the two processes

$$\bar{p}p \rightarrow K_1^0 K^{*0} \quad \Big\lfloor\!\!\rightarrow K^{\pm}\pi^{\mp} \qquad 500 \pm 50 \text{ events},$$

$$\bar{p}p \rightarrow K^{\pm}K^{*\mp} \quad \Big\lfloor\!\!\rightarrow K_1^0\pi^{\mp} \qquad 300 \pm 30 \text{ events}.$$

So, with isospin interference effects, we are able to reproduce the dissymmetry between the production of the two K*, the $K^{*\pm}$ being less abundant than the K^{*0} (figs. 6 and 7).

It is not straightforward to deduce from these results, obtained for the annihilations $\bar{p}p \rightarrow K_1^0 K^{\pm}\pi^{\mp}$, the total transition rate for the K*(891) production in the three-body annihilations in general $\bar{p}p \rightarrow K\bar{K}\pi$.

To the four possible initial states, $\epsilon = \pm 1$, $I=0$ or 1 correspond the four isospin states and transition rates for the production of K*(891):

$$\varphi^{\epsilon}_{0,\frac{1}{2}} = \tfrac{1}{2}[(K^+K^{*-} - K^0\bar{K}^{*0}) + \epsilon(K^-K^{*+} - \bar{K}^0K^{*0})], \quad f^{\epsilon,0}_{K^*K} \qquad (38)$$

$$\varphi^{\epsilon}_{1,\frac{1}{2}} = \tfrac{1}{2}[(K^+K^{*-} + K^0\bar{K}^{*0}) + \epsilon(K^-K^{*+} + \bar{K}^0K^{*0})], \quad f^{\epsilon,1}_{K^*K}. \qquad (39)$$

Let us first consider the two channels corresponding to the states (38), i.e. when $I=0$. In this case, as shown in the appendix (eq. A.5) the wave function $\varphi^{\epsilon}_{0,\frac{1}{2}}$ is identical to $\Phi^{\epsilon}_{0,1}$, being symmetric for $\epsilon = +1$ and antisymmetric for $\epsilon = -1$ in the exchange of the two particles K, $\bar{K}$. Of course, the states with $I(K\bar{K}) = 0$ do not contribute to $\varphi^{\epsilon}_{0,\frac{1}{2}}$; therefore it is possible, in this case, to deduce the total annihilation rates from the observations made on the reaction $\bar{p}p \rightarrow K_1^0 K^{\pm}\pi^{\mp}$ where $I(K\bar{K}) = 1$. Taking into account the visibility of the K_1^0, the weight of the events and the Clebsch-Gordan coefficients explicited in eq. (A.2), one deduces from the observed number of events for $^1S_0$, $I=0$ and $^3S_1$, $I=0$ initial states the produced number of events and the total annihilation rates $f_{K^*K}{}^{+0}$ and $f_{K^*K}{}^{-0}$ given in table 6.

Let us now consider the two channels corresponding to the states (39), i.e. when $I=1$. In this case, as is shown by the relation (A.6), $\varphi^{\epsilon}_{1,\frac{1}{2}}$ is related, not only to $\Phi^{\epsilon}_{1,1}$, but also the $\Phi^{\epsilon}_{1,0}$. The reaction (1): $\bar{p}p \rightarrow K_1^0 K^{\pm}\pi^{\mp}$, for which $I(K\bar{K}) = 1$, provides information only on the part of the state corresponding to $\Phi^{\epsilon}_{1,1}$, i.e. on the symmetric part of the state when $\epsilon = -1$ and the antisymmetric part when $\epsilon = +1$. To reach the other parts of the K* production, we have to observe other channels: the explicit expression of $\varphi^{\epsilon}_{1,\frac{1}{2}}$ given in (A.3) shows that the antisymmetric part of the wave function, when $\epsilon = -1$, will be given by the observation of the channels $\bar{p}p \rightarrow K^+K^-\pi^0$ and $\bar{p}p \rightarrow K_1^0K_2^0\pi^0$, whereas the symmetric part of the wave function, when $\epsilon = +1$, will be given by the observation of the channels $\bar{p}p \rightarrow K^+K^-\pi^0$ and $\bar{p}p \rightarrow K_1^0K_1^0\pi^0$. In table 6, we give the annihilation rates $f^{+,1\,\text{antisym}}_{K^*K}$ and $f^{-,1\,\text{sym}}_{K^*K}$ corre-

sponding to the observed number of events for the channel $\bar{p}p \to K_1^0 K^{\pm}\pi^{\mp}$.

Since the total interference effects between the symmetric and antisymmetric amplitudes amounts to zero when integrated over the all Dalitz-plot, the total annihilation rates $f^{+,1}_{K^*K}$ and $f^{-,1}_{K^*K}$ may be written:

$$f^{+,1}_{K^*K} = f^{+,1\ \text{antisym}}_{K^*K} + f^{+,1\ \text{sym}}_{K^*K} \quad , \tag{40}$$

$$f^{-,1}_{K^*K} = f^{-,1\ \text{antisym}}_{K^*K} + f^{-,1\ \text{sym}}_{K^*K} \quad . \tag{41}$$

In sect. 9, we shall be able to estimate $f^{+,1\ \text{sym}}_{K^*K}$ from the observation of the channel $\bar{p}p \to K_1^0 K_1^0 \pi^0$, therefore the total annihilation rate $f^{+,1}_{K^*K}$ will be given. But for $f^{-,1}_{K^*K}$ we give only a lower limit, (corresponding to $f^{-,1\ \text{antisym}}_{K^*K} = 0$), since the channels $\bar{p}p \to K_1^0 K_2^0 \pi^0$ and $\bar{p}p \to K^+K^-\pi^0$ have not been analyzed.

The values obtained for the masses and widths of the K^{*0} and $K^{*\pm}$ are the following:

$$M(K^{*0}) = 889 \pm 5 \text{ MeV} \ , \quad \Gamma(K^{*0}) = 43 \text{ MeV} \ ,$$

$$M(K^{*\pm}) = 896 \pm 5 \text{ MeV} \ , \quad \Gamma(K^{*\pm}) = 43 \text{ MeV} \ .$$

The complexity of the three-body annihilations $\bar{p}p \to K_1^0 K^{\pm}\pi^{\mp}$, with the presence of at least ten amplitudes, some of them giving rise to strong interference effects, makes the interpretation of the small mass difference observed between the K^{*0} and $K^{*\pm}$ very difficult. We prefer not to attach any significance to this difference.

9. STUDY OF THE REACTION $\bar{p}p \to K_1^0 K_1^0 \pi^0$ (364 events)

The relation (10) of sect. 3 shows that two amplitudes A^+_{01} and A^+_{10} may contribute to the annihilation $\bar{p}p \to K_1^0 K_1^0 \pi^0$.

The first of these amplitudes, A^+_{01}, has been already discussed when analysing the reaction $\bar{p}p \to K_1^0 K^{\pm}\pi^{\mp}$, with the results (table 2) that A^+_{01} leads to the presence of K*(891), $K\bar{K}$(1000), $K\bar{K}$(1280) and S-wave $I = \frac{1}{2}$ Kπ background. These properties of A^+_{01} must be reproduced in the annihilation $\bar{p}p \to K^0 K^0 \pi^0$ if our analysis of the annihilation $\bar{p}p \to K^0 K^{\pm}\pi^{\mp}$ is correct.

In addition, the annihilation $\bar{p}p \to K_1^0 K_1^0 \pi^0$ may exhibit the properties of A^+_{10}, which leads eventually to the presence of the known $I = 0$ $K\bar{K}$ resonances like the S*(1050) and the f⁰(1250), but can also contribute to the presence of some of the K*(891) and S-wave Kπ background.

Our experimental information on the $K_1^0 K_1^0 \pi^0$ system is too limited to attempt a general fit on the Dalitz plot (fig. 17), with all the contributions mentioned above, as it has been done for the $K_1^0 K^{\pm}\pi^{\mp}$ system. Therefore, in a first step, we simply verify that our experimental information on the $K_1^0 K_1^0 \pi^0$ system is in agreement with the properties of the A^+_{01} amplitude

as deduced from the study of the $K_1^0K_1^{\pm}\pi^{\mp}$ system.

The Dalitz plot (fig. 17) shows, at least qualitatively, that this agreement is possible: we observe an accumulation of events in the K*(891) region, leading to a significant peak on the $M^2(K\pi)$ projection (fig. 18). The corresponding decay angular distribution (fig. 19) seems to be compatible with $\cos^2\theta$ apart from background contributions. Moreover, we observe an accumulation of events in the $K\bar{K}(1280)$ region, with an angular distribution characteristic of $J=2$ (figs. 20-22). The background is not uniform: it is more important near the edges of the Dalitz plot, as expected for an S-wave $K\pi$ scattering length effect. However, there is *a priori* no clear evidence of an accumulation of events in the $K\bar{K}(1000)$ region.

However, a quantitative verification of this agreement shows that A_{01}^{+} is not sufficient to reproduce all the features of the $K_1^0K_1^0\pi^0$ system. We have then introduced the A_{10}^{+} contributions to which the quality of the fit is the more sensitive: the K*(891), and the S-wave $K\pi$ scattering length, both with $I_{K\pi} = \frac{1}{2}$ and $I_{K\pi} = \frac{3}{2}$.

In this fit, we have kept the A_{01}^{+} contributions constant, using the values deduced from the study of the $K_1^0K^{\pm}\pi^{\mp}$ system (the K_1^0 visibility and Clebsch-Gordan coefficients lead to a factor $\frac{1}{6}$ for the rates observed in the $K_1^0K_1^0\pi^0$ system compared to the $K_1^0K^{\pm}\pi^{\mp}$). Moreover, the scattering lengths widths and mass values of the Breit-Wigner are also taken from the results obtained for the $K_1^0K^{\pm}\pi^{\mp}$ system.

Table 7 gives the results obtained for the three possible solutions presented in sect. 4. Solutions (iii) and (i) give the best results. They show that the properties of the $K_1^0K_1^0\pi^0$ system are compatible with the interpretation given for the annihilation $\bar{p}p \rightarrow K_1^0K^{\pm}\pi^{\mp}$.

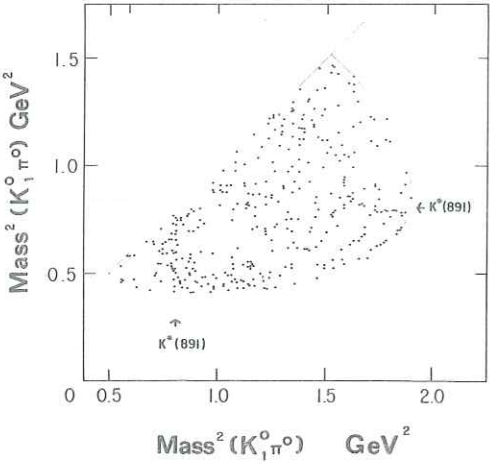

Fig. 17. Folded Dalitz-plot for $\bar{p}p \rightarrow K_1^0K_1^0\pi^0$ (364 events). The region of the K*(891) is indicated by the arrows.

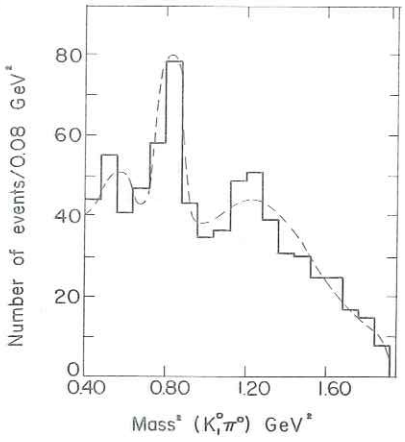

Fig. 18. $(K_1^0\pi^0)$ effective mass squared distribution for $\bar{p}p \rightarrow K_1^0K_1^0\pi^0$ (two combinations per event). The curve represents the theoretical distribution as given by the best fit (solution (iii) of table 7).

Table 7
The parameters ρ and φ

Channel	Amplitude	ρ	φ	Number of events	
Solution (i). $\chi^2 = 60$. $\langle\chi^2\rangle = 39$. $a_{\frac{3}{2}} \neq 0$					
K*		0.53[a]	0.00[a]	25	K*0; M=895 MeV, Γ=45 MeV
S-wave Kπ $I_{K\pi}=\frac{1}{2}$	A^+_{01}	1.19[a]	0.78[a]	130	
K$\bar{K}$(1280)		0.68[a]	0.86[a]	42	K$\bar{K}$(1280); M=1280 MeV, Γ=90 MeV
K$\bar{K}$(1000)		0.81[a]	-0.61[a]	60	K$\bar{K}$(1000): M=1016 MeV, γ=200 MeV
K*		0.48	-0.85	21	
S-wave Kπ $I_{K\pi}=\frac{1}{2}$	A^+_{10}	1.52	-2.00	210	$a_{\frac{1}{2}}(K\pi) = 0.3$ fm
S-wave Kπ $I_{K\pi}=\frac{3}{2}$		2.30	2.09	450	$a_{\frac{3}{2}}(K\pi) = -0.3$ fm
Solution (ii). $\chi^2 = 87$. $\langle\chi^2\rangle = 41$. $a_{\frac{3}{2}} = 0$					
K*		0.62[a]	0.00[a]	33	
S-wave Kπ $I_{K\pi}=\frac{1}{2}$	A^+_{01}	1.16[a]	1.71[a]	117	K*0; M=895 MeV, Γ=40 MeV
K$\bar{K}$(1280)		0.70[a]	1.06[a]	42	K$\bar{K}$(1280); M=1280 MeV, Γ=90 MeV
K$\bar{K}$(1000)		0.48[a]	3.19[a]	20	K$\bar{K}$(1000); M=1016 MeV, γ=200 MeV
K*		0.22	-0.69	4	$a_{\frac{1}{2}}(K\pi) = -0.4$ fm
S-wave Kπ $I_{K\pi}=\frac{1}{2}$	A^+_{10}	0.82	2.36	58	$a_{\frac{3}{2}}(K\pi) = 0$
Solution (iii). $\chi^2 = 55$. $\langle\chi^2\rangle = 39$. K$\bar{K}$(1000) scattering length					
K*		0.63[a]	0.00[a]	35	K*; M=895 MeV, Γ=40 MeV
S-wave Kπ $I_{K\pi}=\frac{1}{2}$	A^+_{01}	1.40[a]	0.36[a]	172	K$\bar{K}$(1280); M=1280 MeV, Γ=90 MeV
K$\bar{K}$		0.71[a]	1.27[a]	44	K$\bar{K}$(1000), a_0 = 2 fm
K$\bar{K}$(1000)		0.95[a]	2.01[a]	79	
K*		0.66	5.19	37	$a_{\frac{1}{2}}(K\pi) = +0.3$ fm
S-wave Kπ $I_{K\pi}=\frac{1}{2}$	A^+_{10}	2.08	2.90	350	$a_{\frac{3}{2}}(K\pi) = -0.3$ fm
S-wave Kπ $I_{K\pi}=\frac{2}{3}$		0.69	1.04	40	

a) Taken from the analysis of reaction (1).

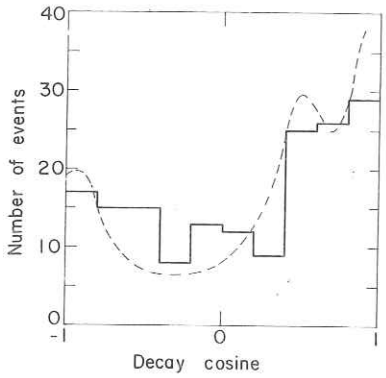

Fig. 19. Decay angular distribution of the K*(891) in $\bar{p}p \to K_1^0 K_1^0 \pi^0$. The curve represents the theoretical distribution as given by the best fit (solution (iii) of table 7).

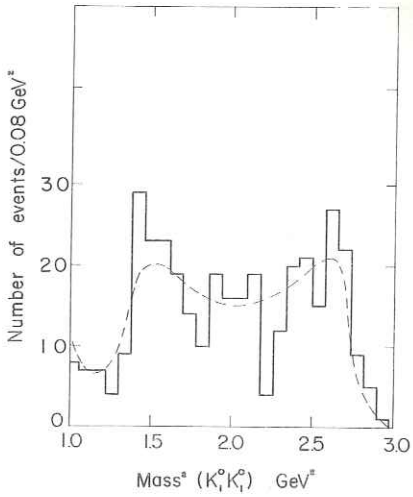

Fig. 20. $(K_1^0 K_1^0)$ effective-mass squared distribution for $\bar{p}p \to K_1^0 K_1^0 \pi^0$. The curve represents the theoretical distribution as given by the best fit (solution (iii) of table 7).

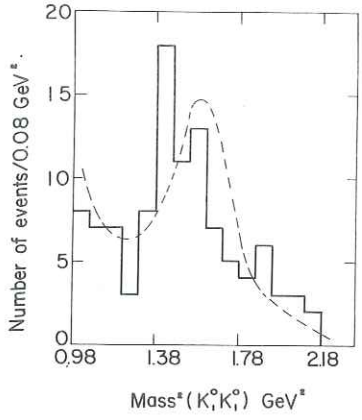

Fig. 21. $(K_1^0 K_1^0)$ effective mass squared distribution for $\bar{p}p \to K_1^0 K_1^0 \pi^0$ when $M^2(K) > 0.9\,\mathrm{GeV}^2$. This cut is to remove the K*(891) reflection. A clear accumulation of events is visible around $1.5\,\mathrm{GeV}^2$ whereas no clear enhancement is visible at threshold. However, the theoretical curve, as given by the best fit (solution (iii) of table 7), gives a reasonable interpretation of the data.

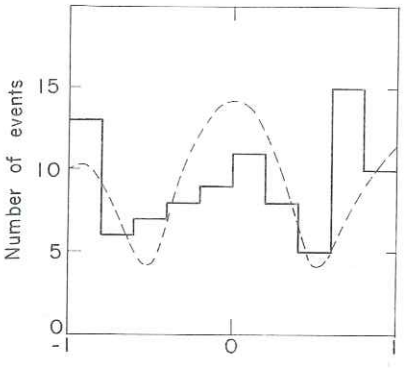

Fig. 22. Decay angular distribution of the $K\bar{K}(1280)$ for $\bar{p}p \to K_1^0 K_1^0 \pi^0$. The curve represents the theoretical distribution as given by the best fit (solution (iii) of table 7), and for spin $J^P = 2^+$ for the $K\bar{K}(1280)$ resonance.

Moreover, they are consistent with a non-negligible production of K*(891) related to the A_{10}^{+} amplitude: 20 ± 10 events, leading to a production rate $f_{K^*K}^{+1\ sym}$ of $(5.35 \pm 2.6) \times 10^{-4}$ as given in table 8.

Table 8
K* production

Initial state	Observed events	Produced events	Rates
$^1S_0\ I=0$	31 ± 5 [a])	950 ± 150 [a])	$f_{K^*K}^{+0} = (8.4 \pm 1.4) \times 10^{-4}$
$^1S_0\ I=1$	20 ± 10	616 ± 308	$f_{K^*K}^{+1\ sym} = (5.35 \pm 2.6) \times 10^{-4}$

[a]) Taken from reaction (1).

Then

$$f_{K^*K}^{+1} = f_{K^*K}^{+1\ antisym} + f_{K^*K}^{+1\ sym} = (6.65 \pm 2.7) \times 10^{-4}. \quad (42)$$

In addition to the results presented in table 8, the study of the $K_1^0K_1^0$ system brings forth the following remarks:

Our data do not show any evidence for the S*(1050) resonance. On the other hand, the $K_1^0K_1^0$ accumulation observed around 1250 MeV is partially explained by the presence of ≈ 40 $K\overline{K}(1280)$ events and the reflection of the K*(891) (the $\cos^2\theta$ angular distribution of the K*(891) leads to two accumulations of events in the $M^2(K_1^0K_1^0)$ spectrum, around 1.5 and 2.6 GeV^2).

However, we cannot completely exclude a small production of f^0, an upper limit for this production with the decay $f^0 \to K^0\overline{K}^0$ being of the order of 10^{-4}.

10. CONCLUSION

A detailed study of the annihilations $\bar{p}p \to K_1^0K^{\pm}\pi^{\mp}$ and $\bar{p}p \to K_1^0K_1^0\pi^0$ at rest shows that several interfering amplitudes play an important role. To give a satisfactory interpretation of the experimental data, we have been led to the introduction of a model, as explained in sect. 3. Three types of interference effects are necessary: the interference of two amplitudes not related by the Bose statistics, a good example of which being the A_2 and the K* resonances. The interference between two amplitudes related by the Bose statistics, like the K* and $\overline{K}$* resonances. The interference between two amplitudes of different total isospin, leading to the disymmetry observed on the Dalitz plot.

We have also shown that it is impossible to reproduce the accumulation observed in the $(K\overline{K})$ system at threshold without the introduction of a specific amplitude. Several interpretations have been proposed, in sect. 5, for

this $I=1$ $K\bar{K}$ enhancement at threshold. One of them is to relate this enhancement to the presence of a narrow $I^G J^P = 1^- 0^+$ resonance around 972 MeV, which could be identified to the δ-meson. However, one cannot exclude other interpretations, like the existence of a new resonance $I^G J^P = 1^- 0^+$ at 1016 MeV with $\Gamma \approx 25$ MeV, or, more simply, the presence of a $K\bar{K}$ amplitude represented by a scattering length of 2 fm with no clear relation to a resonating channel.

The K*(891) production is nearly completely determined, the $^3S_1$, $I=1$ being preponderant, as already shown by Barash et al. (ref. [2]. The annihilation rates $f^{\epsilon I}_{K^*K}$ ($\epsilon = \pm 1$, $I=0,1$) are:

$$f^{+0}_{K^*K} = (8.4 \pm 1.4) \times 10^{-4} , \quad f^{-0}_{K^*K} = (1.7 \pm 1.0) \times 10^{-4} ,$$

$$f^{+1}_{K^*K} = (6.6 \pm 2.7) \times 10^{-4} , \quad f^{-1}_{K^*K} \geqslant (23.4 \pm 2.0) \times 10^{-4} .$$

We have also observed the production of a $K\bar{K}$ resonance with a mass $M = 1280 \pm 12$ MeV and a width $\Gamma \approx 90$ MeV.

Its most probable quantum numbers are $I^G J^P = 1^- 2^+$. These characteristics make its identification with the A_2 meson highly probable.

Its production rates $f^{+0}_{A_2\pi}$ and $f^{-1}_{A_2\pi}$ corresponding respectively to $^1S_0$, $I=0$ and $^3S_1$, $I=1$ initial states are

$$f^{+0}_{A_2\pi} = (6.5 \pm 1.8) \times 10^{-4} , \quad f^{-1}_{A_2\pi} = (2.2 \pm 0.9) \times 10^{-4} .$$

Finally, an important S-wave background (annihilation rate of the order of 40×10^{-4}) may be represented by a small S-wave $K\pi$ scattering length $|a_{K\pi}| < 1$ fm.

We should like to express our thanks to Professors B. Gregory, L. Leprince-Ringuet and J. Teillac for their interest and support, and to Professors R. Armenteros, Ch. Peyrou and J. Prentki for many stimulating discussions.

APPENDIX. ISOSPIN DECOMPOSITION ACCORDING TO THE $K\pi$ COUPLING SCHEME

$$S|\bar{p}p + \epsilon\bar{p}p\rangle = \sum_{I, I_{K\pi}} B^{\epsilon}_{I, I_{K\pi}} |\varphi^{\epsilon}_{I, I_{K\pi}}\rangle , \tag{A.1}$$

where the notations are easily deduced from those of sect. 3,

$$\varphi^{\epsilon}_{0,\frac{1}{2}} = \frac{1}{\sqrt{6}} \{(K^+\pi^-)\bar{K}^0 + (K^0\pi^+)K^- - \frac{1}{\sqrt{2}}((K^+\pi^0)K^- + (K^0\pi^0)\bar{K}^0)$$

$$+ \epsilon [(K^-\pi^+)K^0 + (\bar{K}^0\pi^-)K^+ - \frac{1}{\sqrt{2}}((K^-\pi^0)K^+ + (\bar{K}^0\pi^0)K^0)]\} , \tag{A.2}$$

$$\varphi^{\epsilon}_{1,\frac{1}{2}} = \tfrac{1}{2}\{(K^+\pi^0)K^- - (K^0\pi^0)\bar{K}^0 + \epsilon((K^-\pi^0)K^+ - (\bar{K}^0\pi^0)K^0)\}\,, \qquad (A.3)$$

$$\varphi^{\epsilon}_{1,\frac{3}{2}} = \tfrac{1}{2}\{(K^+\pi^-)\bar{K}^0 - (K^0\pi^+)K^- + \epsilon((K^-\pi^+)K^0 - (\bar{K}^0\pi^-)K^+)\}\,, \qquad (A.4)$$

?

when we compare these expressions with those obtained for $\Phi^{\epsilon}_{I,I_{KK}}$ in sect. 3, one verifies directly that

$$\varphi^{\epsilon}_{1,\frac{1}{2}} = \Phi^{\epsilon}_{0,1}\,, \qquad (A.5)$$

$$\varphi^{\epsilon}_{1,\frac{1}{2}} = \frac{-1}{\sqrt{3}}\,\Phi^{\epsilon}_{1,0} - \sqrt{\tfrac{2}{3}}\,\Phi^{\epsilon}_{1,1}\,, \qquad (A.6)$$

$$\varphi^{\epsilon}_{1,\frac{3}{2}} = \sqrt{\tfrac{2}{3}}\,\Phi^{\epsilon}_{1,0} - \frac{1}{\sqrt{3}}\,\Phi^{\epsilon}_{1,1}\,. \qquad (A.7)$$

The inverse relations written in sect. 3 are easily deduced. The same relations hold for the amplitudes $A^{\epsilon}_{I,I_{K\bar{K}}}$ and $B^{\epsilon}_{I,I_{K\pi}}$. We can write the transition rates for the reactions (1)-(4) in terms of the amplitudes B:

$$R_1 = \tfrac{1}{9}\left|\sqrt{2}\,B^{+}_{0,\frac{1}{2}} - \sqrt{2}\,B^{+a}_{1,\frac{1}{2}} - B^{+a}_{1,\frac{3}{2}}\right|^2 + \tfrac{1}{9}\left|\sqrt{2}B^{-}_{0,\frac{1}{2}} - \sqrt{2}\,B^{-s}_{1,\frac{1}{2}} - B^{-s}_{1,\frac{3}{2}}\right|^2$$

$$R_2 = \tfrac{1}{27}\left|B^{+}_{0,\frac{1}{2}} - B^{+s}_{1,\frac{1}{2}} + \sqrt{2}\,B^{+s}_{1,\frac{3}{2}}\right|^2\,,$$

$$R_3 = \tfrac{1}{9}\left|B^{-}_{0,\frac{1}{2}} - B^{-a}_{1,\frac{1}{2}} + \sqrt{2}\,B^{-a}_{1,\frac{3}{2}}\right|^2\,,$$

$$R_4 = \tfrac{1}{6}\left|B^{+}_{0,\frac{1}{2}} + B^{+s}_{1,\frac{1}{2}} - \sqrt{2}\,B^{+s}_{1,\frac{3}{2}}\right|^2 + \tfrac{1}{6}\left|B^{-}_{0,\frac{1}{2}} + B^{-a}_{1,\frac{1}{2}} - \sqrt{2}B^{-a}_{1,\frac{3}{2}}\right|^2\,, \qquad (A.8)$$

where R_1, R_2, R_3 and R_4 depend only on the symmetric or antisymmetric part of the $B_{I,I_{K\pi}}$ amplitudes (B^{s} and B^{a}) since the final states (1)-(4) correspond only to the symmetric or antisymmetric part of the states $\varphi^{\epsilon}_{I,I_{K\pi}}$.

The symmetry properties of the states $\Phi^{\epsilon}_{I,I_{K\bar{K}}}$ are given by the G-parity conservation (see sect. 3.2) and those of the states $\varphi^{\epsilon}_{I,I_{K\pi}}$ are deduced from the expressions in terms of the $\Phi^{\epsilon}_{I,I_{K\bar{K}}}$ states.

[1] R. Armenteros et al., Phys. Letters 17 (1965) 170, 344.
[2] N. Barash et al., Phys. Rev. 139 (1965) B1659.
[3] Ch. Zemach, Phys. Rev. 133 (1964) B1201.
[4] J. Duboc, A. Minten and S. Wojcicki, CERN report 65-2.
[5] R. Armenteros et al., Proc. Geneva Intern. Conf. on High energy physics, 1962, p. 90.
[6] R. Armenteros et al., Presented at Oxford Intern. Conf., 1965.
[7] Gillespie, Final State Interactions (Holden-Day advanced physics monographs).
[8] P. Baillon et al., to be published in Nuovo Cimento.
[9] J. Barlow et al, to be published in Nuovo Cimento.
[10] C. Baltay et al., Phys. Rev. 142 (1966) 932.
[11] R. H. Dalitz, Strange particles and strong interactions (Oxford University Press, 1962) p. 59.
[12] R. H. Dalitz, Proc. 1965 Oxford Conf. on High energy physics, p. 162.